NASA CR-159723

LABORATORY MEASUREMENTS IN A TURBULENT, SWIRLING FLOW

David P. Hoult

Massachusetts Institute of Technology
Cambridge, Massachusetts 02139

Prepared for

NATIONAL AERONAUTICS AND SPACE ADMINISTRATION
Lewis Research Center
Cleveland, Ohio 44135

November 1979

Grant NSG-3076

TABLE OF CONTENTS

SUMMARY

This report discusses measurements of soot inside a flame-tube burner using a special water-flushed probe. The soot is measured at a series of points at each burner and upon occasion gaseous constituents NO, CO, hydrocarbons, etc. have also measured. Four geometries of flame-tube burners have been studied, as well as a variety of different fuels. The main results of the report can be put into categories. First, we have studied the role of upstream geometry on the downstream pollutant formation. We have found that the amount of soot formed is particularly sensitive to how areodynamically clean the configuration of the burner is upstream of the injector swirl vanes. Second, we have studied the effect of pressure on soot formation. We have chosen to interpret the main effect of changing pressure as a variation in the Reynolds number of the flow. We have found that beyond a certain Reynolds number, the peak amount of soot formed in the burner is constant. Third, we have studied a variety of different fuels in the burner to determine a relationship between the properties of the fuel and the amount of soot formed. We have found that the hydrogen to carbon ratio of the fuel is a rough indicator of the peak amount of soot formed in the burner--although one can distinguish, in our data, the effects of different fuels having the same hydrogen to carbon ratio. That is, some fuels produce more soot than others even when the hydrogen to carbon ratio is the same. Finally, a discussion of these results in the line of current literature is provided with tentative interpretation of the data.

I. INTRODUCTION

This research has been motivated by a variety of interests. It was recognized [1] that very little firm information is available on the kinetic scheme of soot formation in a typical gas turbine combustor, so that theoretical models of the process, which would necessarily involve uncertainties in turbulence estimates, kinetics, local stoichiometry, and local temperature of the flow, seemed unpromising. Instead, this report discusses a series of experiments, which have arisen as we have more carefully defined the conditions of a laboratory system so that it behaves in a similar fashion to the primary zone of a combustor in a large gas turbine.

The geometry of these experiments has been fixed downstream of the injector. It consists of a fuel injector (air assist, or pressure type atomizer) on the centerline of a circular cross section flame tube. The atomizer is supported by an axisymmetric set of 45° swirl vanes.

Initial efforts were made to develop a reliable sampling system, to measure the soot concentration and polycyclic hydrocarbons (PCAH) in the flow. [2]

Even though the geometry of the burner seemed straightforward, we soon found out this was not the case. [3] The axisymmetric geometry did not produce an axisymmetric mean concentration pattern for soot, O_2, hydrocarbons, CO, etc. A variety of geometric changes were studied; in each soot concentrations were measured. We have

shown that the geometry of the hardware upstream of the burner needs careful design if axisymmetric, uniform concentrations of soot are produced. Section II of this report details the geometries studied.

The results of the purely geometric studies is presented in Section III. In that section we discuss how changes upstream of the burner make substantial changes in the emission generated.

Due to the atmospheric pressure and low velocities used in our first burners, the Reynolds numbers were low, about 5,000, based on hot flow exit conditions. The turbulent properties of the flow could be expected to change with increasing density (pressure), velocity, and size - all of which increase the Reynolds numbers. In Section IV scaling laws for soot formation are presented. These laws are as yet tentative.

In addition, Section IV deals with a variety of results: The location of PCAH compounds in the primary zone; the sooting behavior of benzene - heptane mixtures; the effects of varying stoichiometry on soot formations; and the sooting effects of varying hydrogen/carbon ratios in blends of jet engine fuels.

The long range goal of this research is to be able to reliably simulate, in a laboratory burner, the chemical and fluid processes which occur in a gas turbine combustor. To do this, we have developed preliminary scaling laws discussed in the last section (Section V) which suggest how soot levels vary with fuel and stoichiometery. In the long run, this engineering approach should lead to a better understanding of how to design and adapt combustors to new and changing fuels. [4]

II. GEOMETRIES TESTED

There are four geometries which will be discussed in this study, which we shall label A, B, C and D. Figure 1 shows the geometries A and B. In geometry A, the burner is tubular, 53 cm long, combustion air is supplied at atmospheric pressure, and is passed through 45° stationary swirl vanes. The burner diameter is 12.7 cm. Fuel is supplied through an air assist atomizer (DeLavan model 3060-9-11, see Fig. 2) on the burner axis. The air supply for the atomizer is independent of the main air supply. Perhaps 5% of the total air flow in the burner passes through the atomizer. The atomizing pressures vary from 184 KPa (12 psig) to 239 KPa (20 psig). Ignition is accomplished with a pair of standard oil burner electrodes.

Geometry B is identical to geometry A, except the diameter is 7.6 cm, hence allowing for higher flow velocities, while using the same compressor.

The upstream configuration of geometries A & B is shown in Figure 1. Immediately upstream of the swirl vanes, the pipe diameter is the same as the burner diameter. Within one diameter of the swirl vanes, the fuel and air are fed into an air blast injector through standard plumbing hardware. In the plane of the air and fuel fittings, the blockage in the burner is about 30% of the area of the tube, for the 7.6 cm diameter burner.

Geometry C is the same as Geometry B downstream of, and including, the swirl vanes and atomizer. However, upstream of the swirl vanes, the pipe diameter is 15.2 cm, so the blockage due to fittings is about 1/4 that of Geometry C. In addition, the main air flow passes through a large settling chamber before entering the pipe section. See

Figure 3. This system can be run premixed by evaporating fuel in the settling chamber at a known rate, as well as operating in the standard heterogeneous mode.

Geometry D is a 7.6 cm diameter tube burner, with 45° swirl vanes, using a pressure injector. The fittings, upstream of the swirl vanes, used to carry fuel to the nozzle are specially designed and fabricated, and consist of aerodynamically streamlined struts positioned some 3 diameters upstream of the nozzle. Fuel flows through the struts to a tube, located on the centerline, and hence to the nozzle. Geometry D is capable of being pressurized to about 7 atmospheres. The mass flow rate is controlled by a sonic orifice downstream of the flame tube. See Figure 4.

Gas and soot samples in each of these geometries are collected using a unique, water flushed probe. Figure 5 shows this probe,[2] which, when it is used to collect soot, is flushed by part of the cooling water flowing down the center tube. The probe flush water is turned off when gas samples are taken, but small amounts of leakage prevent reliable measurements of water vapor to be made.

The soot collected is deposited on a fiberglass filter, which is desiccated and then weighed to determine the amounts of soot collected. As the sampling flow rate is known, the resulting figure can be translated into soot mass concentrations inside the burner.

The gas concentrations measured, CO, CO_2, NO_x HC and O_2 are measured by commercially available instruments mounted on a gas cart.

III. GEOMETRIC EFFECTS

The first indication of the complexity of the flow came from measurements of the contours of soot in geometry B. Typical examples are shown in Figure 6, which gives the estimated soot contours 2 diameters downstream of the swirl vanes and injector. It is seen that the soot pattern is very far from axisymmetric. For this soot pattern, the injector was an air assist atomizer using Kerosene run with 15 psig atomizing pressure, and fuel equivalence ratio of 1.0. Study of the gradients in soot closer to the burner produced the data shown in Figure 7 taken along one radius, (θ fixed in cylindrical polar coordinates) for Z/D = 1.33.

Since we wished to determine if this effect was repeatable, without the long data collection time for soot measurements ($\sim$ 3 hours/data point), we measured gas concentrations (CO, CO_2, NO_x, O_2 and hydrocarbons). An informative way to plot the data is to use the water gas equilibrium constant (Fig. 8) to reduce the measured concentrations to values of ϕ. The results of repeated runs is shown in Figure 9 at Z/D of 1.33. Although there is about a 15% scatter in the data, the effect is clearly reproducible. Apparently, the rich area of the flow is formed near the injector. But the effects of the nonuniformity are reflected in nonuniform soot concentrations some distance downstream.

To define this effect further, the upstream end of geometry B was rebuilt, as described in the previous section. In this geometry C, we compared the maximum centerline value of soot concentration (at about Z/D = 1.5) for the B and C geometries. This is shown in Figure 10 for benzene. An additional feature of the geometry C is the ability to run premixed,[5] this condition is also shown for heptane in Figure 11.

Keeping in mind that the geometry and flows through the injector and swirl vanes are identical in the old geometry (B) and the new geometry (C) in Figure 10, we can see that substantial differences in soot level can be caused by different upstream geometries.[5, 3] The injector remained in place during the premixed tests. The fact that premixing reduced the soot levels to zero over the range $0.4 < \phi < 1.6$ is consistent with thermodynamic equilibrium calculations which suggest that no solid carbon should exist at these values of ϕ, and that soot formation is related, in some way, to the non-uniform mixing of fuel and air.

Turning now to geometry D, the nonuniformity in soot was controlled by careful attention to aerodynamic detail upstream of the nozzle and swirl vanes. Figures 12, 13 and 14 show measured values of soot[6] for various positions. These data indicate that the soot and ϕ pattern is axisymmetric if both the upstream and downstream geometry is axisymmetric.

In geometry D we made a special study of the role of the blockage such as could be caused by an upstream obstruction. In the aerodynamically clean geometry which gave the results shown in Figures 12, 13 and 14, we deliberately changed the upstream geometry by placing a blockage plate over one of the swirl vanes (shown schematically in Figs. 15 and 16).

In performing tests[7] to determine the role of this blockage, a limited test grid was set up, comprising of a measurement along the center line of the burner and measurements at four azimuthal angles, $\theta = 0°$, 90°, 180° and 270°, at a radius of 2.5 cm. The sampling grid went from 1½ diameters downstream of the injector to 2, 2½ to 3, 4, 5, 6

and 7 diamaters downstream. A large number of data points were generated. To cut down on the collection time, measurements of the value of ϕ were determined through exhaust gas sampling - which is much faster than soot collection.

It's convenient in summarizing this data to extract from the data the data points which show the effect of the blockage from those which do not. The data points which show the effect of the blockage are called anomolous points. The figures which we show next separate the anomolous data points from the other data points. That is, only a few measured values in each cross section look unusual when only one vane of the swirl is blocked. All the other points are called normal. For example, in Figure 17 we show ϕ at a radius of 2.5 cm, for various Z/D, the normal data points as a function of axial location both with the blockage plate in and the blockage plate out. The value of ϕ the first rises and then levels off at about Z/D = 4. The final value, ϕ = .8, for Z/D greater than 4, is the overall stoichiometry of the burner. In the next figure, Figure 18, the same data is shown for the center line. The center line starts very rich, because at Z/D = 1, the fuel spray is very rich on the burner axis. Again by Z/D = 4, the flow has become well mixed to the extent that the center line value of ϕ is essentially the same as that of the inflow fuel and air. [These values of ϕ are determined using the water gas reaction in the measurements of gas constituents.]

Excluding the anomolous points, Figure 19 shows the oxygen concentration as a function of distance downstream and one can see that for $Z/D \geq 4$ the equilibrium (corresponding to ϕ of 0.8) oxygen concentration of about 4% is obtained.

We now can ask how far downstream the nonuniformity due to blockage persists. This has to do with the anomalous data points. For example, in the next figure, Figure 20,

we show the value of ϕ for various azimuthal positions of the probe location at Z/D = 5. Although the error bars overlap at θ = 90°, 180°, and 270° they do not at θ = 0°. The error bars are from a number of repeated points. From this we can conclude that at 5 diameters there is an effect of blockage which can be seen in the contours of stoichiometry. A similar result occurs for all diameters less than 5. The final figure in this section, Figure 21, shows that at 6 diameters, all the data points essentially overlap. Other data show the same thing for Z/D of 7. Although the grid is not fine enough to determine whether the nonuniformity rotates with the supposed hot flow swirl velocity set up by the swirl vanes, the data do support the conjecture that the nonuniformity persists a substantial distance, 5 diameters, downstream. Within the accuracy of the data, it is between 4 and 5 diameters downstream that the flow becomes well mixed.

These data support the idea that a nonuniformity upstream can generate a defect or a change in stoichiometry which persists until combustion is essentially complete.

IV. CHEMICAL EFFECTS

The first measurements of chemical constituents in the turbulent, swirling flow characterized the soot formation process in the geometries which we presently label A and B. These results were reported by Prado, et al [2] in 1976. The essential result will only be summarized here. Figures 22 and 23 show the soot concentration of geometries A and B respectively, (Figures 2 and 3 of Prado, et al). Compare these results with Figure 24 showing the concentration of PCAH (Figure 4, [2]). Polycyclic hydrocarbons, (PCAH), were found closer to the nozzle or injector than the peak in soot concentration. In analyzing the structure of PCAH some 30 cyclic compounds were identified, with the molecular weight increasing with distance from the nozzle. In geometries A and B, where Prado, et al., got their results, the flow is nonuniform due to the geometry upstream of the swirl vanes, and the Reynolds numbers are small, an effect which will discussed in a moment.

The next study of chemical effects was done in geometry [8] C. The peak amount of soot formed on the axis is shown in Figure 25 for a variety of benzene - heptane mixtures. The point shown on this chart, "Kerosene", is so located that its C to H ratio matches that of the appropriate benzene - heptane mixture. One can see that there is substantial difference between the peak amount of soot formed from benzene - heptane mixture and from Kerosene, at the same C to H ratio. The Reynolds number of the flow is low, as this burner operated at atmospheric pressure.

Another chemical effect which is important is that of stoichiometry. Our current understanding of the role of the overall stoichiometry of the burner runs something like this. Only a fraction of the eddies in the flow form soot. In particular, if the burner is

running with an overall equivalence ratio of near 1, there will be some probability distribution of ϕ for each eddy, around the mean value of the stoichiometry. From thermodynamic calculations, we believe that only eddies which are richer than a stoichiometry of 2 will form soot. Hence, only a small fraction of the eddies in the flow are rich enough. However, as the overall value of ϕ is varied toward the richer side there will be a larger and larger fraction of eddies rich enough to form soot. This effect shown in Figure 26 for geometry B.[8] It is interesting and instructive to compare this result with that of MacFarlane [9] which is shown on the same curve. MacFarlane's data was taken at 6 atmospheres whereas the data shown in Figure 26 was taken at atmospheric pressure. One can see that there is not a major difference between the two results even though MacFarlane's geometry was not the same as geometry B.

We now turn to the results of chemical effects which we obtained in geometry D, [6] the pressurized burner. Our first efforts were directed to the following experiment: The burner was run at a fixed overall stoichiometry of 1.25 with Kerosene as a fuel. The upstream and downstream geometry of the burner was held fixed. In this system the pressure of the burner was changed systematically by changing the size of the sonic orifice downstream. In this way the Reynolds number of the flow was changed due to the changing density of the flow. We then ask how the peak value of soot varies with pressure or Reynolds number. These results are shown in Figure 27. The middle two points in the chart are for the same injector but the data point at a Reynolds number of approximately 12,000, and the point at the Reynolds number approximately 3,500 are for two other injectors. However, this initial result seems to suggest that above a certain Reynolds number, the peak amount of soot formed was independent of Reynolds number. Each plotted point is the average of about 3 - 6 measurements. The accuracy is $\pm$ 10%.

To remove the effect of changing injectors, the same experiment was repeated using propane flowing out through a jet coaxial with the center line of the burner in the same location as the liquid fuel injector. In this experiment there was no change in the Reynolds numbers, swirl numbers, or geometry over the range of pressures studied.

The results are shown in Figure 28 and it is clear that there is a leveling off at a certain Reynolds number on the order of 15,000. These results imply an absence of pressure scaling of the peak soot loading. This is contrary to the results of MacFarlane [9] (1974), a point which we will take up in the discussion.

Figure 29 and 30 and all the remaining figures in this section deal with measurements made at Reynolds numbers high enough to be in the range where the peak amount of soot is independent of Reynolds number. In Figure 29 and 30 we show four different fuels, Jet A, Decaline, Tetralin, and Xylene. Notice that the peak value of soot is always at the same location in the burner. Within the accuracy of the data, the rise from Z/D = 0 to the peak value of soot and the subsequent decay afterwards has essentially the same slope, for the different fuels. For these reasons, both the data in Figures 29 and 30 and also in the preceding two charts are use only the peak value of soot as an indicator of the total behavior of soot in the burner.

The last chart shows the peak loading of soot scaled with percent hydrogen by weight for the various blends tested. It is commonly believed that the C to H ratio is a good way to scale the amount of soot formed for different fuels (10) and this figure, Figure 31, supports that idea. However, one can see from the data that there is difference between the amount of soot formed and the character of the blend. We believe that

these closely related blends might be typical of what would get from broad spec fuels, such as the ERBS [11] fuel. Hence, if one scales entirely by percent hydrogen one could imagine the different fuels would give somewhat different levels of soot in a given combustor.

V. DISCUSSION OF RESULTS

The major part of this discussion will be centered around the interpretation of the Reynolds number scaling presented in the previous section. However, it should be emphasized at the outset that these data are not complete because the variation with Reynolds number was achieved only with a variation in pressure. Ideally, these experiments need to be repeated in which a given Reynolds number was achieved by varying either flow rate or pressure. In the experiments which we report the pressure and flow rate were varied simultaneously rather than independently.

We start by attempting to make a nondimensional argument for how the flow geometry and combustion process in the burner might scale. A number of the important nondimensional parameters are known. First of all, there is the stoichiometry

$$\phi = \frac{\text{mass flow fuel/mass flow air}}{(\text{mass flow fuel/mass flow air})/_{\text{stoichiometric}}} \qquad (1)$$

Typically, in our experiments, ϕ varies from 1.5 to 0.6. However, in the section on chemical effects, most of the ϕ values were near 1.

A second scaling parameter is a Reynolds number: the ratio of viscous to inertial forces. It is known from standard non-reacting flows that the Reynolds number is important in determining the turbulent motions of the flow. When the Reynolds number of a flow is high enough the large scale turbulent mixing processes no longer depend on viscousity. That is, the turbulent diffusivity for the large scale eddies is Reynolds number independent. For a pipe flow with no reactions, the friction on the wall does not vary Reynolds number for $Re > 10\text{-}20{,}000$.

$$Re = \rho UD/\mu \qquad (2)$$

In present experiments the Reynolds number ranged from a few thousand for geometries A, B and C up to approximately 20,000 in various circumstances for geometry D.

Another important nondimensional number characterizing the flow is the swirl number. Tnis number has been described by Beer [12] and is a ratio of the angular momentum to the axial momentum going through the swirl vanes. Its definition is (see Beer, Sec. I.I)

$$S = \frac{2}{D}\int_0^R (W)\ U\pi 2\ rdr \Big/ \int_0^R \rho U 2\pi r dr \qquad (3)$$

A typical value for the swirl number in all the experiments reported in this report is 0.8. Varying the swirl number changes the amount of recirculation just downstream of the injector swirler geometry.

Fuel properties are more difficult to scale. First of all, there may be many reactions for different parts of the combustion process and, secondly, different fuels may have different reaction schemes. However, the hydrogen to carbon ratio has been suggested by the results of Section IV as a parameter. It is simply the percentage weight of hydrogen to the percentage weight of carbon in the fuel. We know that this scaling is not completely correct because different fuels which have the same C to H ratio give slightly different results. However, the early results shown in Figure 25 on benzene - heptane mixtures in geometry C should not be interpreted as a lack of hydrogen to carbon scaling of soot loading. Those first experiments were done at too low a Reynolds number. For the want of a better scheme, we shall assume that X scales the fuel properties.

$$X = \frac{\text{mass Hydrogen}}{\text{mass Carbon}}, \quad \% \qquad (4)$$

Finally, we can make an estimate of the ratio of the flow time divided by the reaction time to form soot. To estimate the reaction time, we look up low pressure data for burners which has been summarized by Prado [1]. These data show a time of about 1 millisecond to reach a peak soot concentration in a laminar flow burner at 20 tor. We shall assume that the soot reaction time scales inversely with pressure, as does the flame thickness. This is based on the fact that the soot seems to be formed at the same relative position in the laminar flame, independent of pressure (1). Using this estimate, we can calculate the nondimensional ratio of the flow time to the reaction time.

$$\tau = \frac{\text{flow time}}{\text{reaction time}} = \frac{1}{10^{-3}\text{sec.}} \frac{760\ \text{mmHg} \cdot 5\ \text{atm D}}{(20)\text{mmHg}\quad U} = 10^3 \qquad (5)$$

This calculation indicates the flow time or turbulent mixing time is much longer than the reaction time. This supports the idea that the turbulent mixing process controls the amount of soot formed. Hence that there should be a Reynolds number scaling of the soot, as the mixing process scales with Re.

However, we have no definitive argument about why the peak values of soot should or should not scale with pressure. MacFarlane's [9] data, which suggests a strong pressure dependence of soot amount, is somewhat deficient in this regard because, in the same paper, he showed that the flow geometry of his burner system changes with pressure. As we have found, (Sec. III) small changes in geometry can make major changes in the amount of soot formed. However, MacFarlane's data can be contrasted with the data of Kadota et al [13] for droplet burning, at various pressures.

They show that when the ambient pressure of the atmosphere around the drop rises to the point where the burning wake of the droplet becomes turbulent, the mass of soot produced from burning a droplet essentially remains constant as the pressure is further increased. Although the present work does not refer to droplet burning, a similar scaling effect may occur in our fully turbulent flow.

If it turns out that future studies confirm the scaling suggested here, interesting possibilities for the practical application of this similitude, based on the five nondimensional numbers listed, seem important. For example, it might be possible, by setting up an appropriately scaled swirler and injector, to simulate the amount of soot formed one or two diameters downstream of the swirler in a full scale engine.

REFERENCES

(1) J. Lahaye and G. Prado, "Mechanisms of Carbon Black Formation", Chemistry & Physics of Carbon, Editors, Philip Walker and Peter Thrower, 14, pp 167-294, (1978)

(2) G. Prado, M. L. Lee, R. A. Hites, D. P. Hoult and J. B. Howard, Soot and Hydrocarbon Formation in a Turbulent Diffusion Flame" 1976, pp 649 - 661, 16th International Symposium on Combustion.

(3) D. P. Hoult, "Soot Formation in a Turbulent Swirling Flow" pp 309 - 321, 1977 NASA Conference on Aircraft Engine Emissions, NASA Conference Publication 2021.

(4) See, for example; H.F. Butze and F. M. Humenek, "Parametric Performance of a Turbojet Engine Combustor Using Jet A and a Diesel Fuel", NASA TM 78089, March 1979.

(5) B. Irani, "Effects of Reynolds Number and Mixing on Soot Production in a Turbulent Diffusion Flame", August 1977, MS Thesis in Mechanical Engineering, MIT, Cambridge, Mass.

(6) J. A. Hoover, "Soot Production in a Turbulent Diffusion Flame: Turbulent Scaling and Fuel Composition Effects", June 1978, MS Thesis in Mechanical Engineering, MIT, Cambridge, Mass.

(7) J. D. Savino, "The Effect of an Upstream Air Blockage on a Continuous Oil Combustor Emissions", May 1978, BS Thesis in Mechanical Engineering, MIT, Cambridge, Mass.

(8) K. Shamsavari, "Measurement of Soot in a Turbulent Diffusion Flame", July 1976, MS Thesis in Mechanical Engineering, MIT, Cambridge, Mass.

(9) F. H. Holderness and J. J. MacFarlane, "Soot Formation in Rich Kerosene Flames at High Pressure", Atmospheric Pollution by Aircraft Engines, AGARD Cp. No. 125, 18 - 1, (1973).

(10) R. P. Lohman, E.J. Szetela, and A. Vranos, "Analytic Evaluation of the Impact of Broad Specification Fuels on High By-pass Turbofan Engine Combustors", December 1978, NASA CR-159454.

(11) J. P. Longwell, "Jet Aircraft Hydrocarbon Fuels Technology", NASA CP-2033, 1978.

(12) N. Syred and J. M. Beer, "Combustion in Swirling Flows: A Review", Combustion & Flame, 23, pp 143 - 201 (1974).

(13) T. Kadota, H. Hiroyasu and A. Farazandehmehr, "Soot Formation by Combustion of a Fuel Droplet in High Pressure Gaseous Environments", Combustion & Flame 29, pp 67 - 75, (1977).

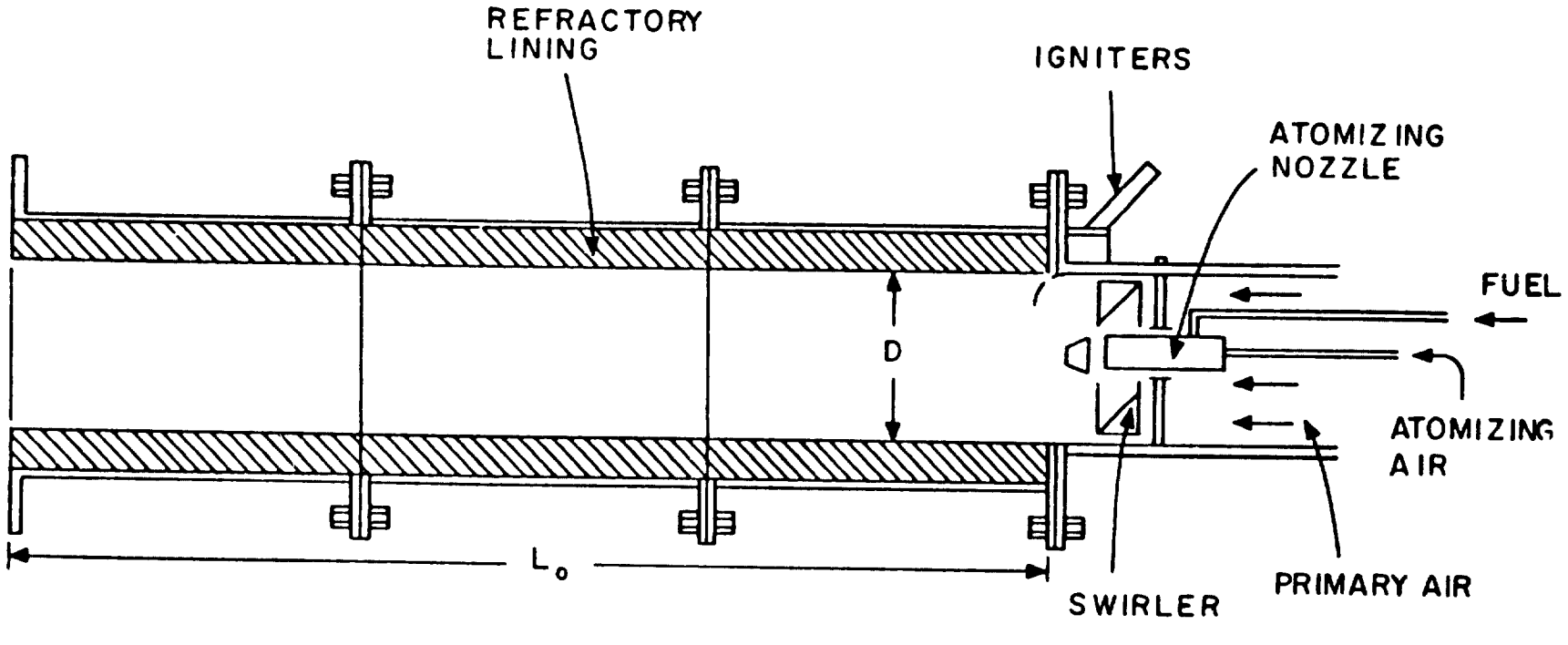

Fig. 1 Schematic of Burner Cross Section, Configurations A and B.

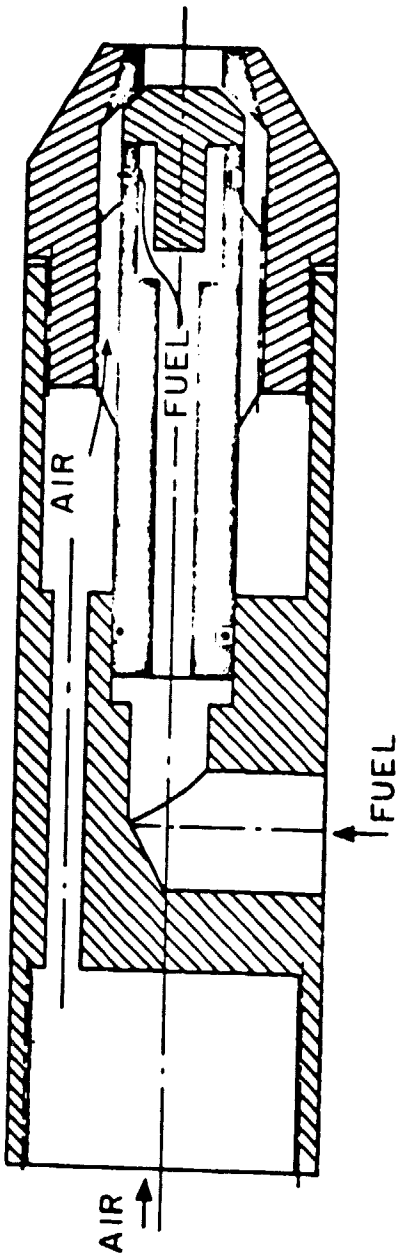

Fig. 2 Schematic Cross Section of the Air-Assist Atomizer Used in Configurations A, B and C.

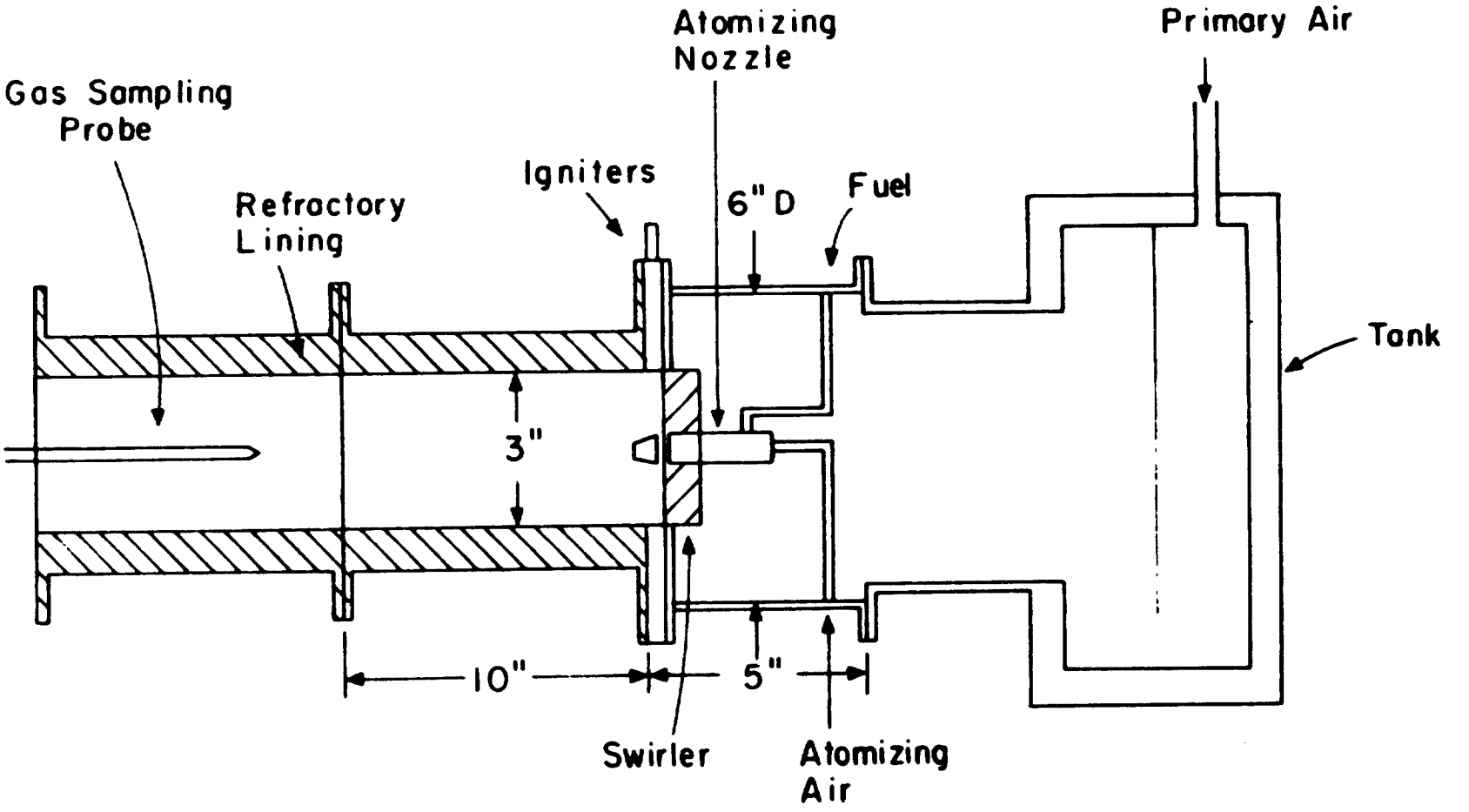

Fig. 3 Schematic of Burner Cross Section, Configuration C.

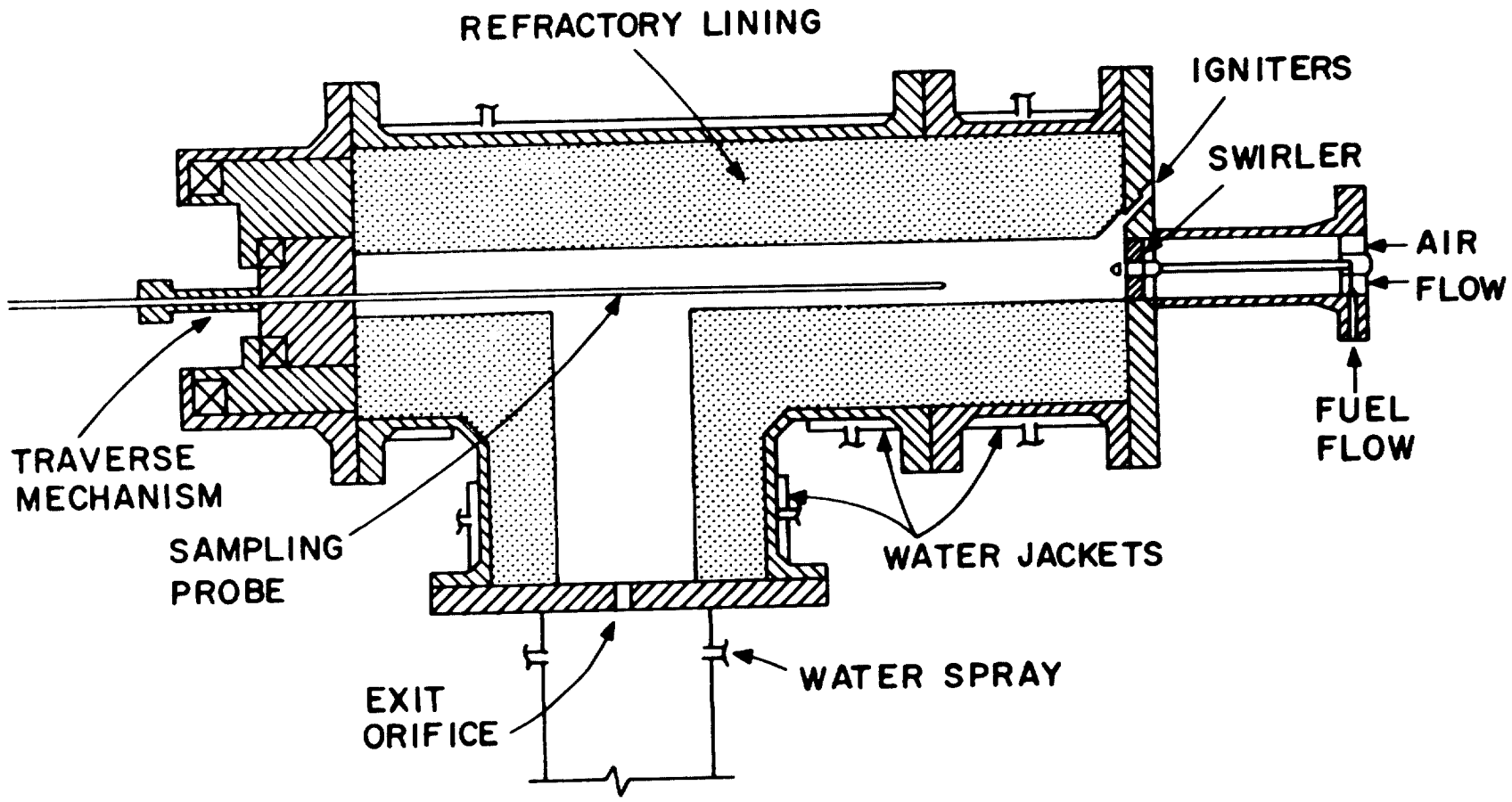

Fig. 4 Schematic Cross Section of High Pressure Burner, Configuration D.

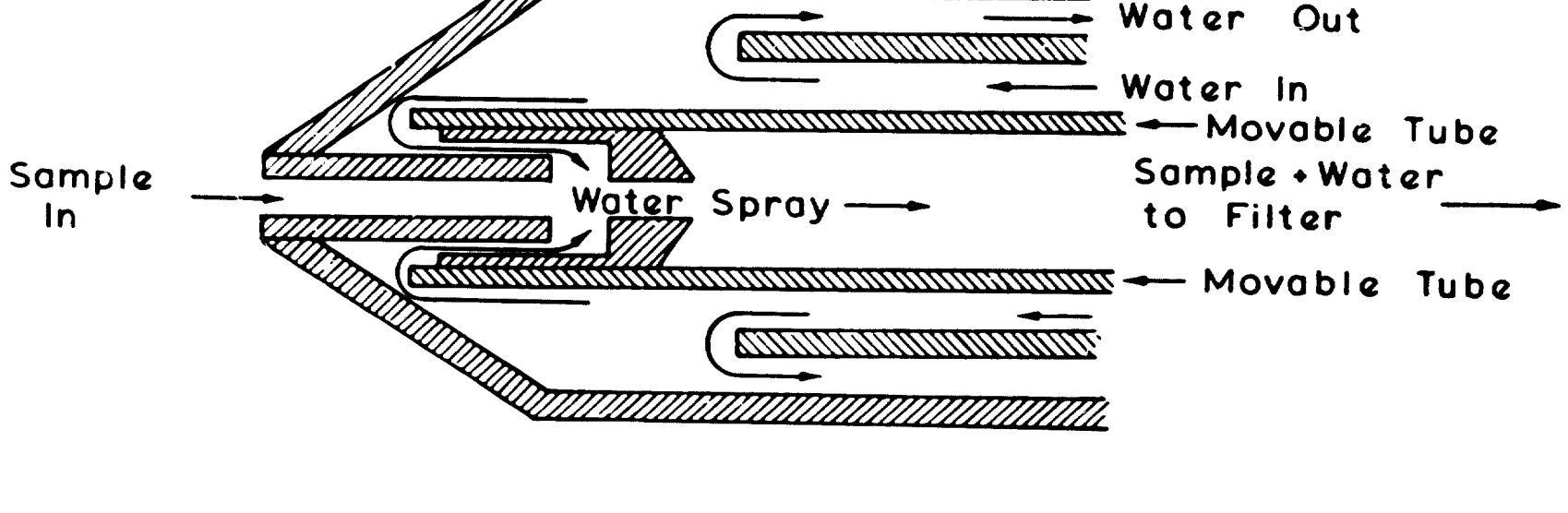

Fig. 5 Schematic of the Tip of the Cooled, Water-Flushed Soot Sampling Probe.

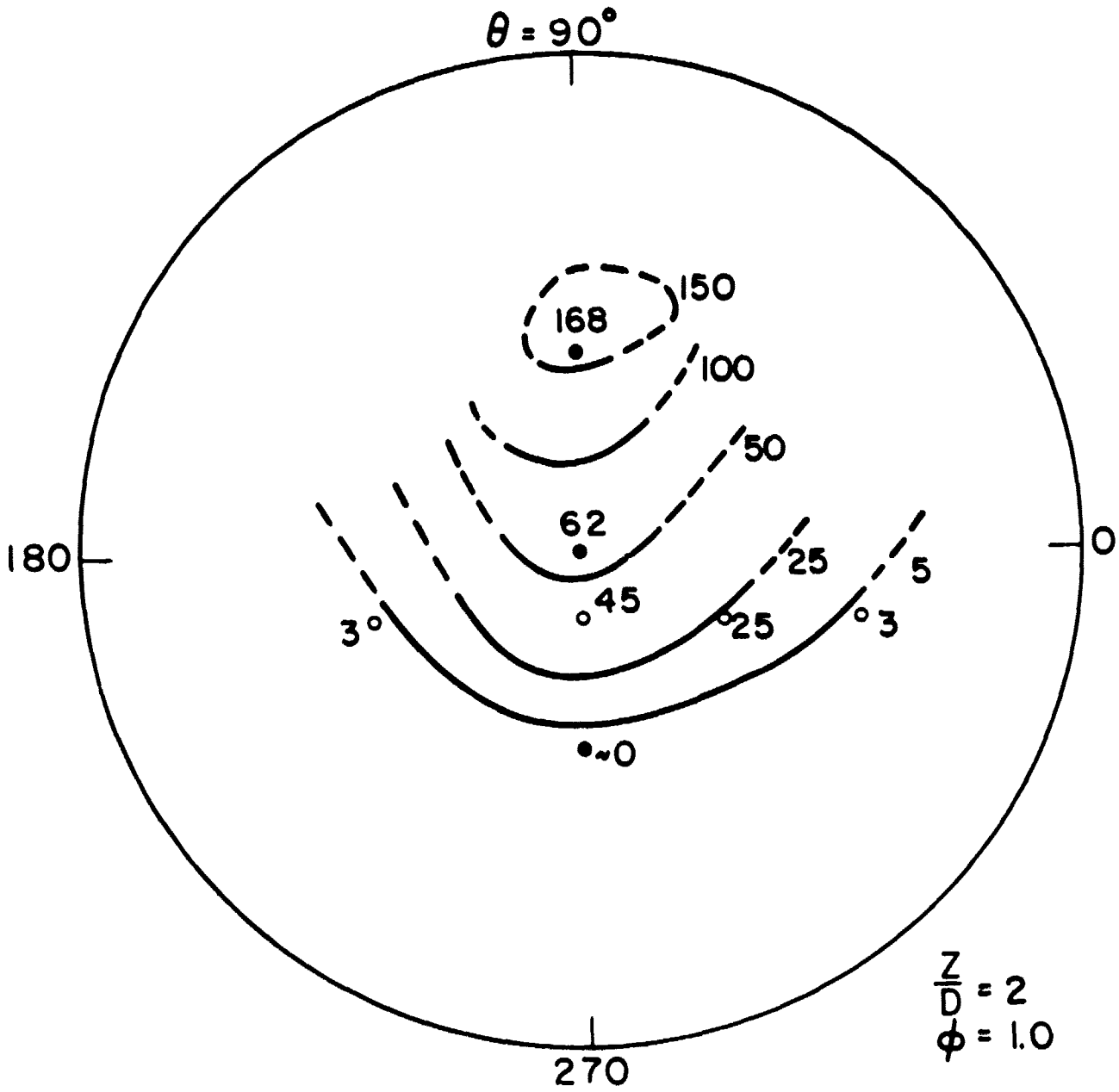

Fig. 6 Distribution of Soot-Loading at a Position Two Burner Diameters Downstream of Fuel Injector, Configuration B.

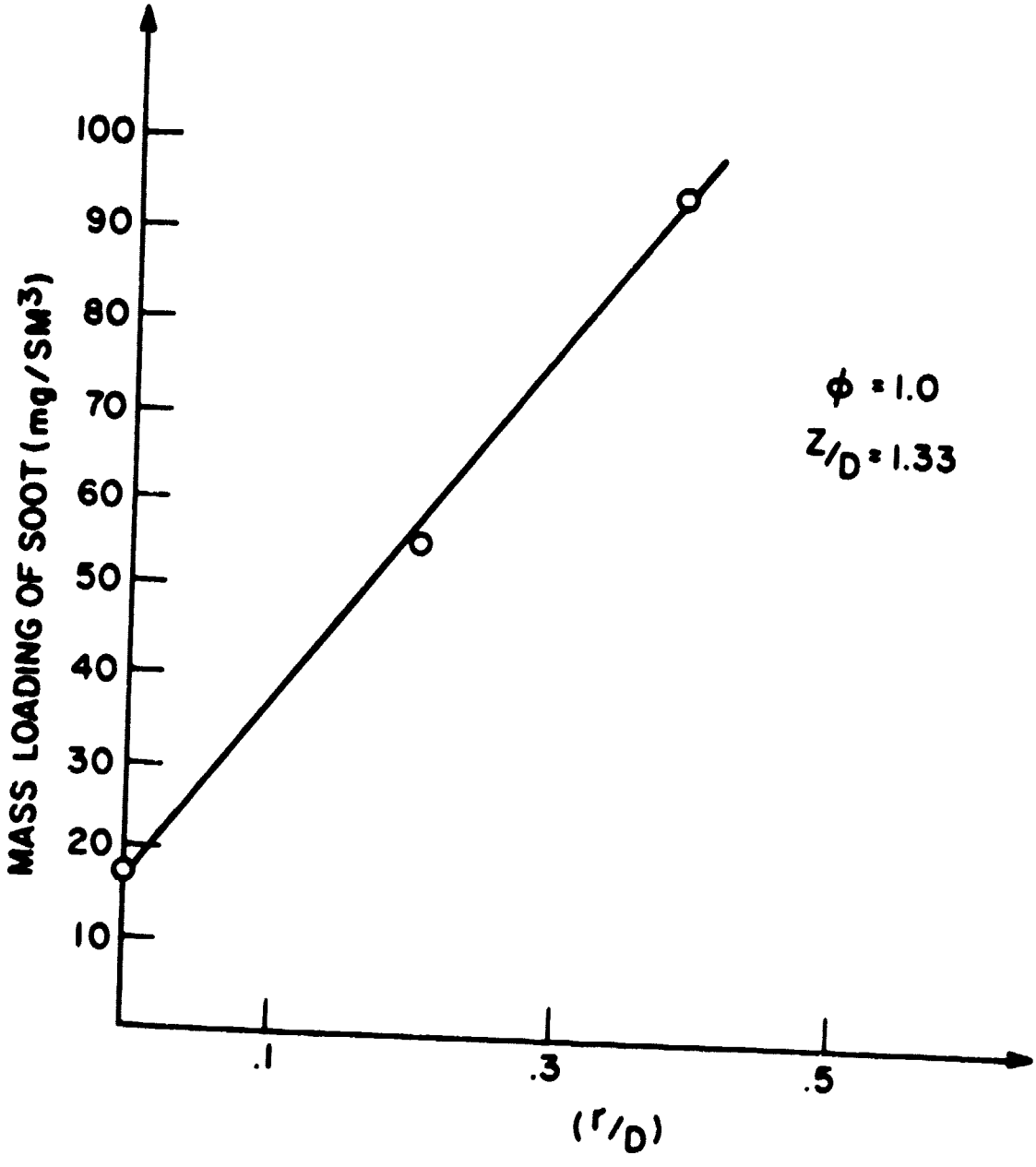

Fig. 7 Variation of Soot Loading in the Radial Direction in a Plane Located at 1.33 Diameters Downstream of Injector, Configuration B.

Calculation of equivalence ratio, ϕ, from

Values of $[NO_x]$, $[CO]$, $[CO_2]$, $[HC]$, and $[O_2]$

Equation of combustion

$$\phi\, C_xH_yO_z + 4.76\,(Air) \rightarrow A_1CO + A_2CO_2 + A_3H_2O + A_4H_2 + A_5O_2 + A_6C_rH_s + A_7[NO_x]$$

Measured: Dry concentrations of CO, CO_2, O_2, & NO_x
Wet concentration of HC

Goal: Calculate equivalence Ratio, ϕ

Method and Assumptions:

—Water-gas equilibrium constant

$$K = \frac{A_1A_3}{A_2A_4} = 3.8$$

—Calculate $[H_2O]$ using $[CO]$ & $[CO_2]$ and K.

—Wet concentrations found from dry concentrations

$$[\quad]_w = [\quad]_D\,[1 - [H_2O]\,]$$

—For HC $\quad \frac{x}{y} = \frac{r}{s}$

Fig. 8 Method of Determining Equivalence Ratio of Sampled Gas as a Function of Species Concentrations.

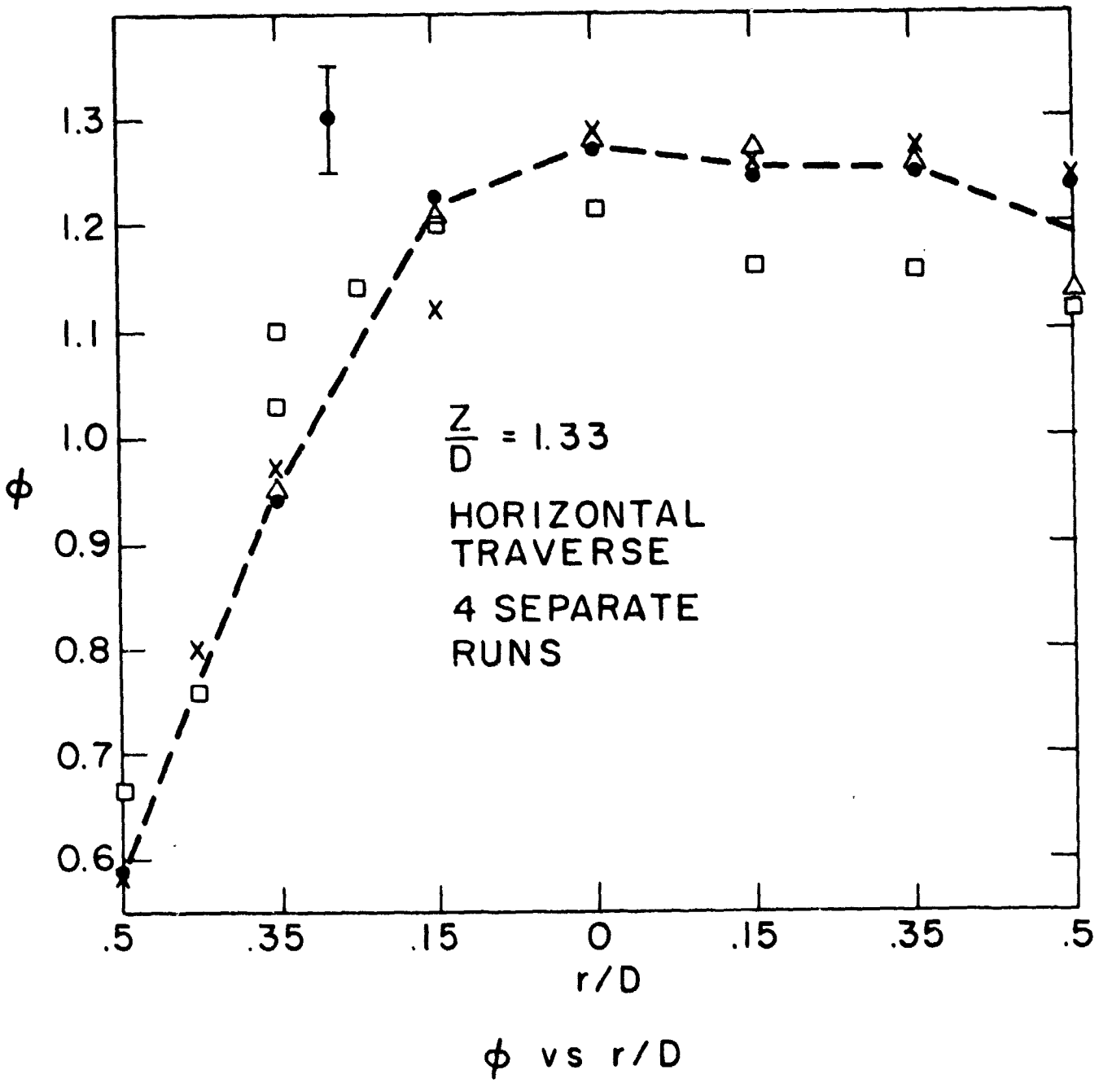

Fig. 9 Variation of Equivalence Ratio in the Radial Direction in a Plane Located at 1.33 Diameters Downstream of Injector, Configuration B.

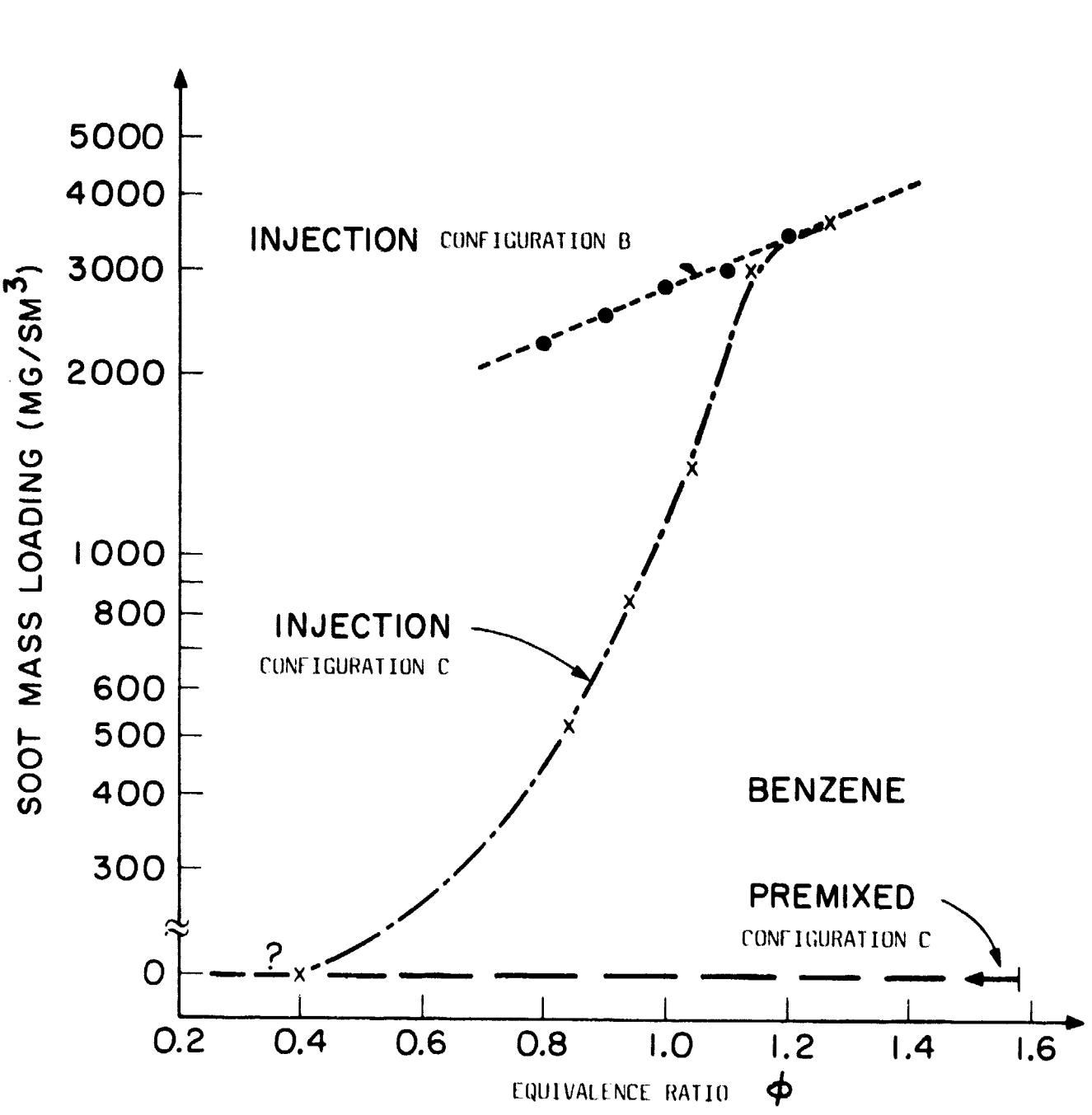

Fig. 10 Variation of the Centerline Soot Loading as a Function of Equivalence Ratio at 1.5 Diameters Downstream of the Injector, Configurations B and C.

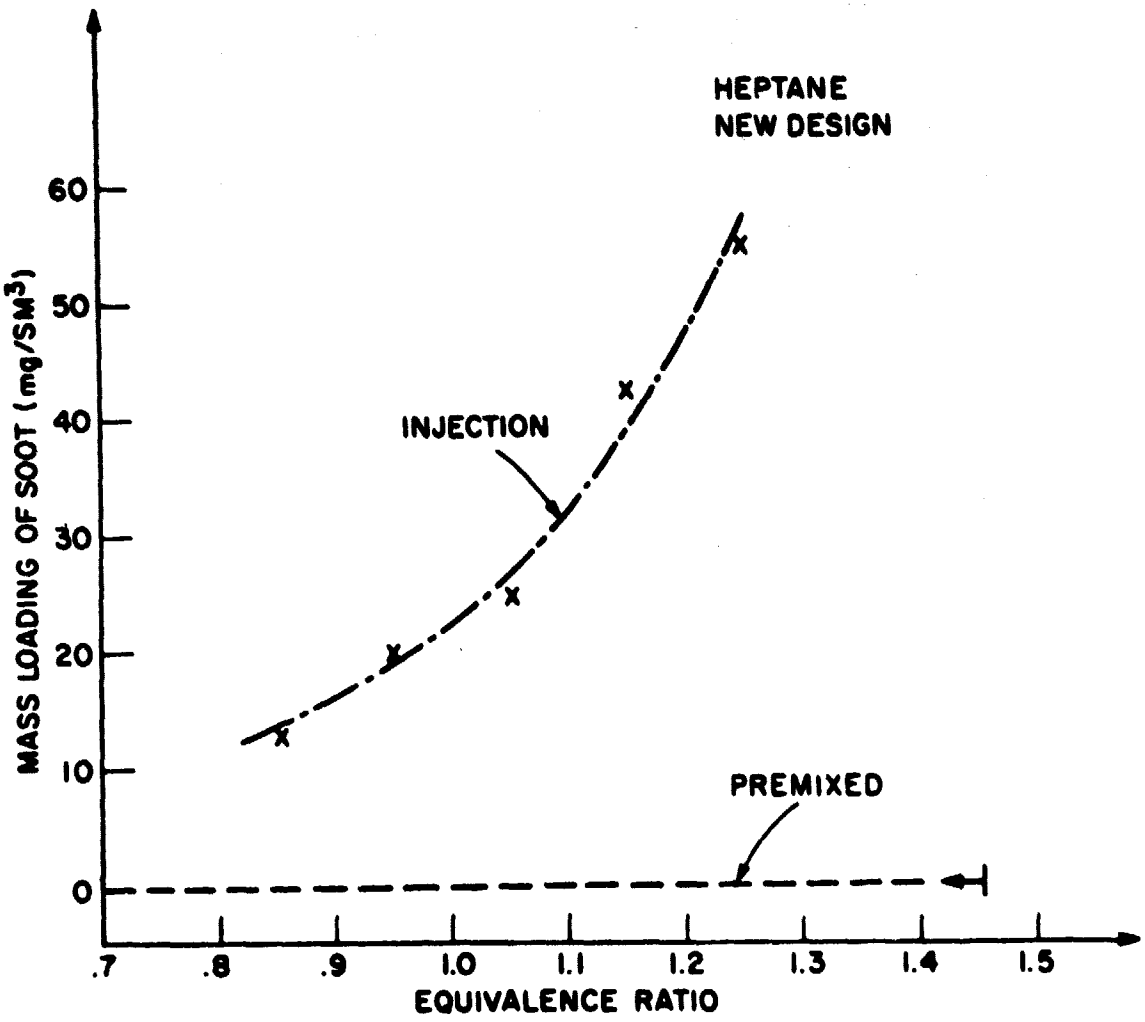

Fig. 11 Variation of the Centerline Soot Loading for Heptane as a Function of Equivalence Ratio at 1.5 Diameters Downstream of the Injector, Configuration C.

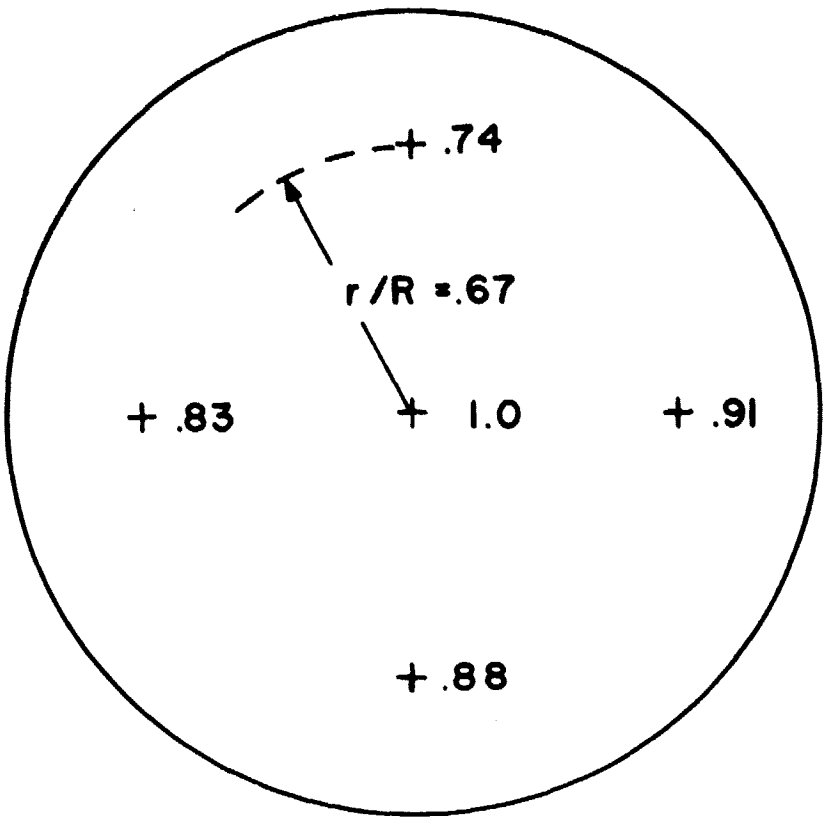

FUEL: JETA

ϕ = .8

Re = 17,450

Z/D = 2.5

SOOT LOADINGS

NORMALIZED:

1.0 = 1850 mg/Sm^3

R = 3.8 cm

Fig. 12 Distribution of Soot Loading at a Position 2.5 Diameters Downstream of Injector, an Axial Location of Peak Soot Loading, Configuration D.

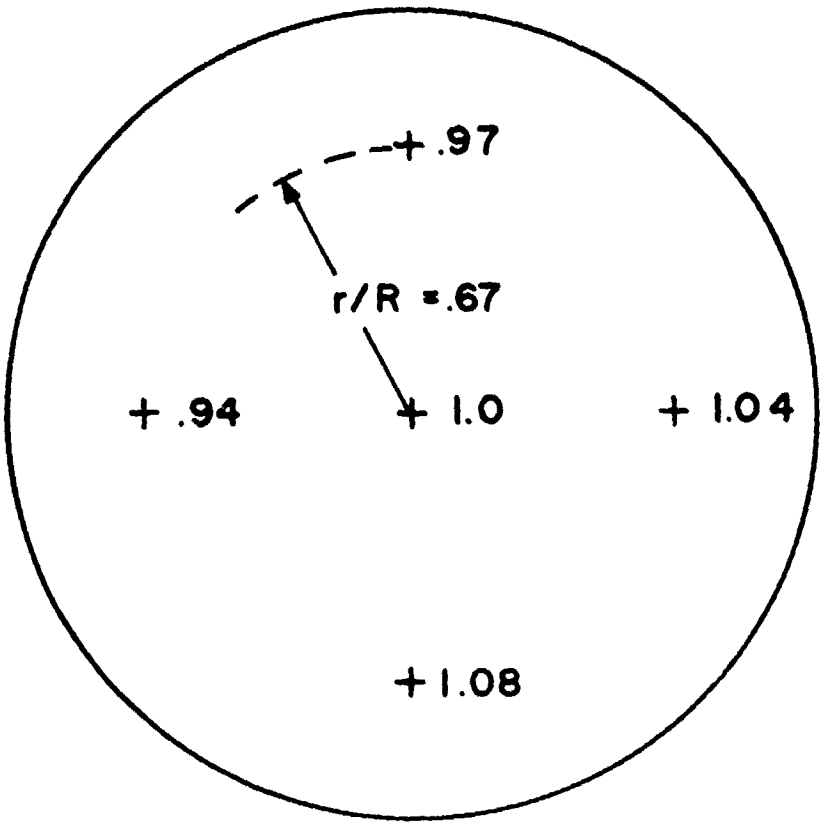

FUEL: JETA

ϕ = .8

Re = 17,450

Z/D = 4.0

SOOT LOADINGS NORMALIZED:

1.0 = 1650 mg/Sm^3

R = 3.8 cm

Fig. 13 Distribution of Soot Loading 4.0 Diameters Downstream of Injector, Configuration D.

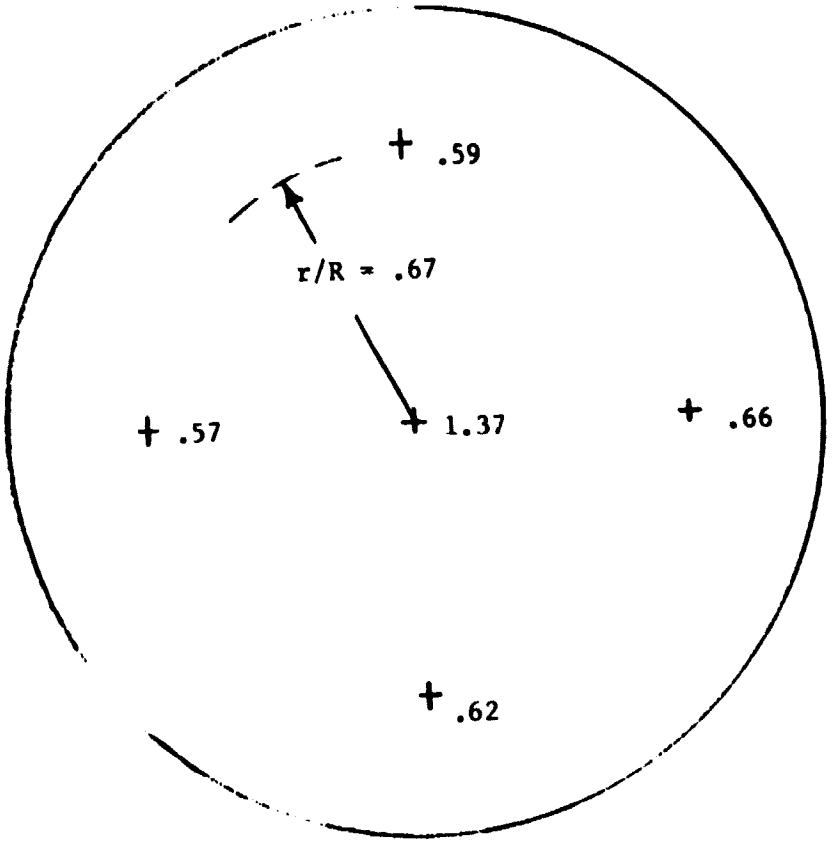

Fuel: Jet A

$\phi_{overall}$ = .8

Re = 17,450

R = 3.8 cm

Z/D = 1

Fig. 14 Distribution of Soot Loading One Diameter Downstream of Injector, Configuration D.

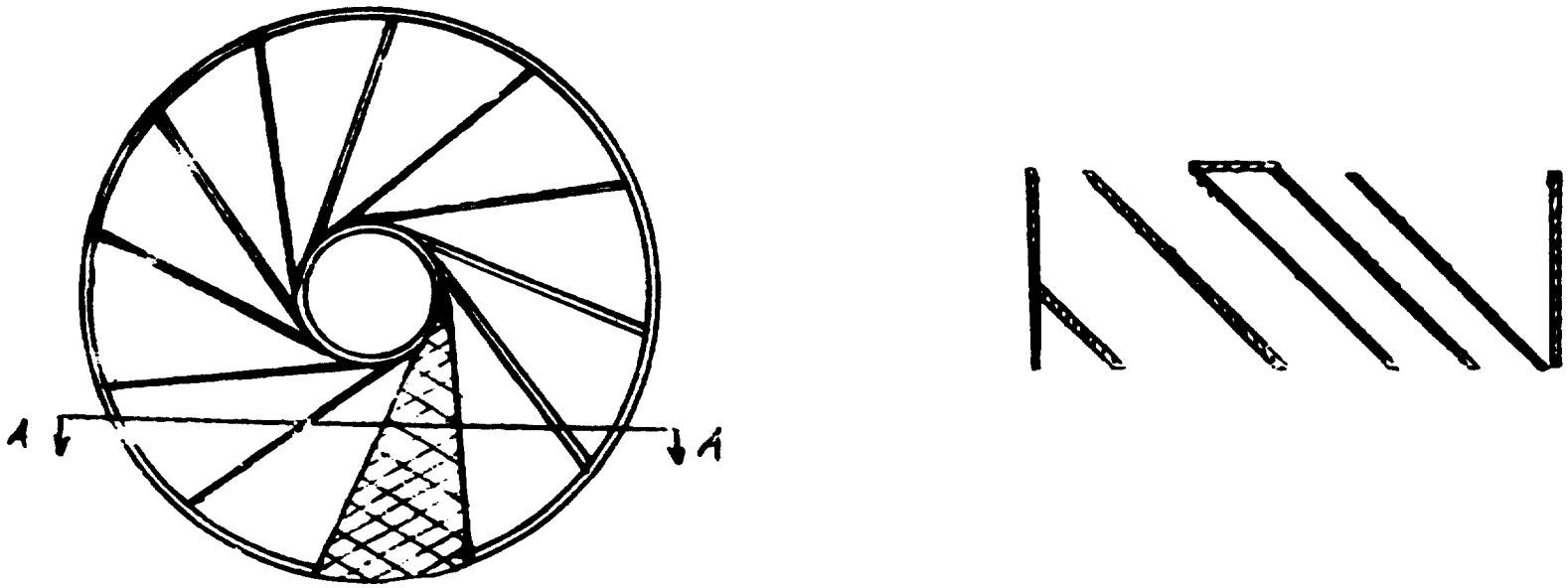

Fig. 15 Schematic Showing Location of the Blockage Plate on the Swirler Vanes.

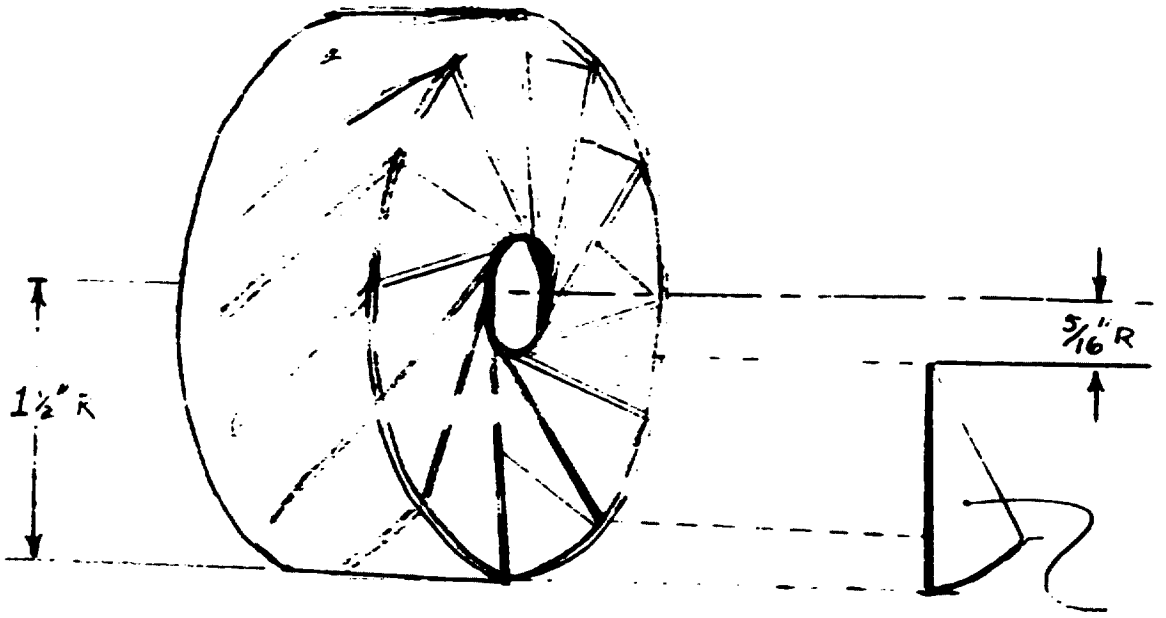

Fig. 16 Assembly Diagram of the Swirler Vanes and Blockage Plate.

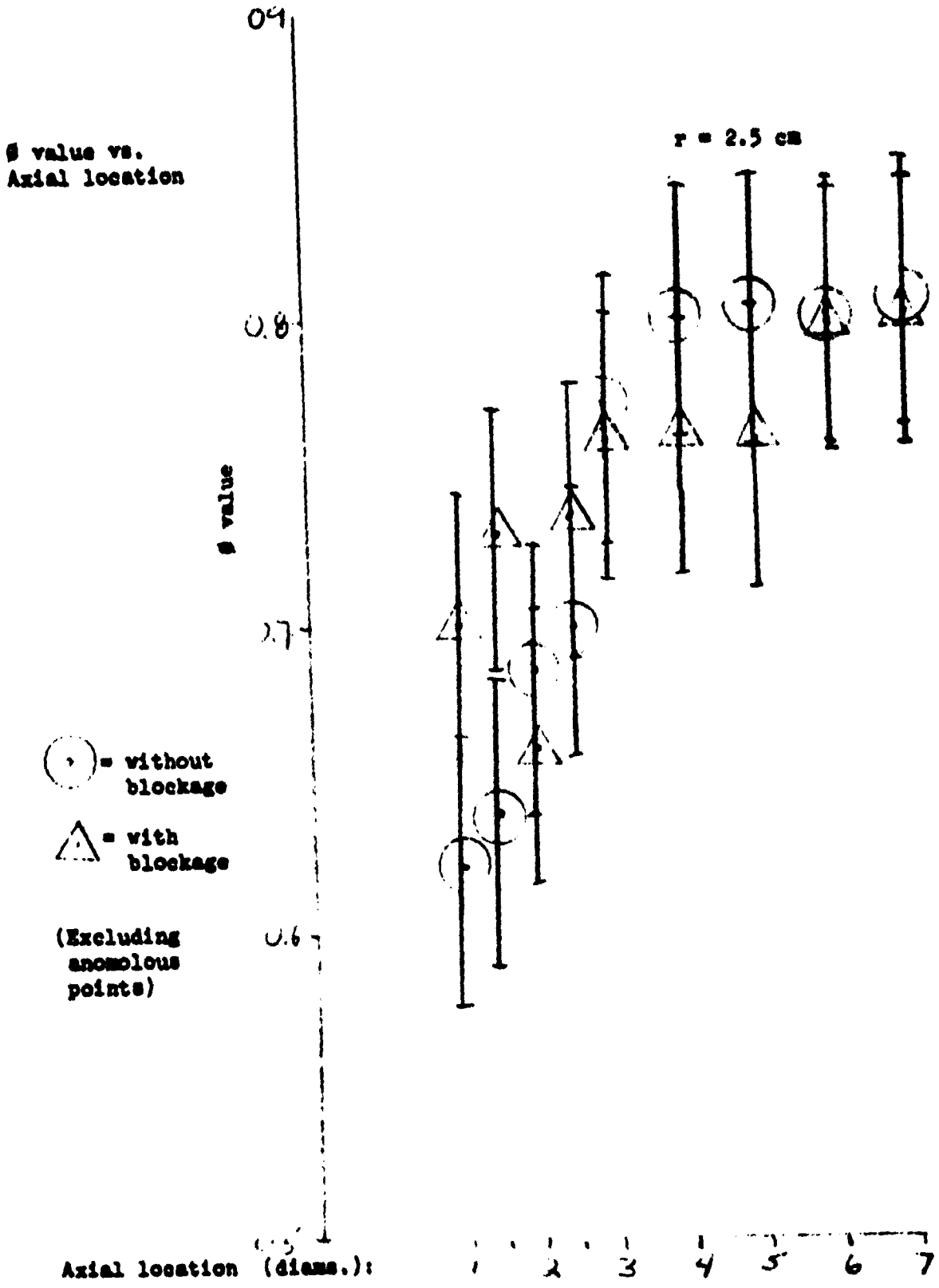

Fig. 17 The Variation of Equivalence Ratio at a Radius of 2.5 cm as a Function of Axial Location for Cases With and Without Blockage, Configuration D.

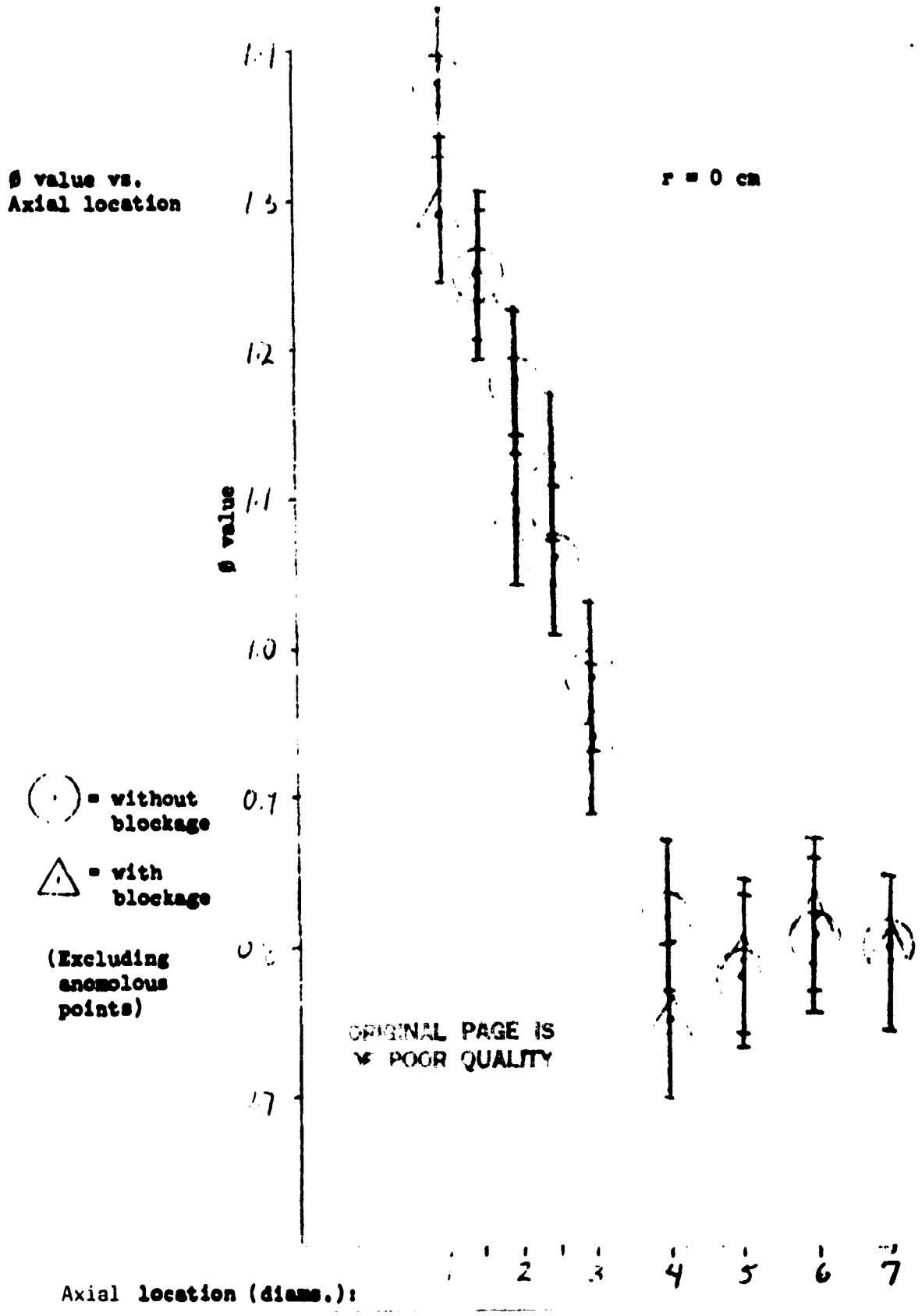

Fig. 18 The Variation of Equivalence Ratio at the Centerline of the Burner as a Function of Axial Location for Cases With and Without Blockage, Configuration D.

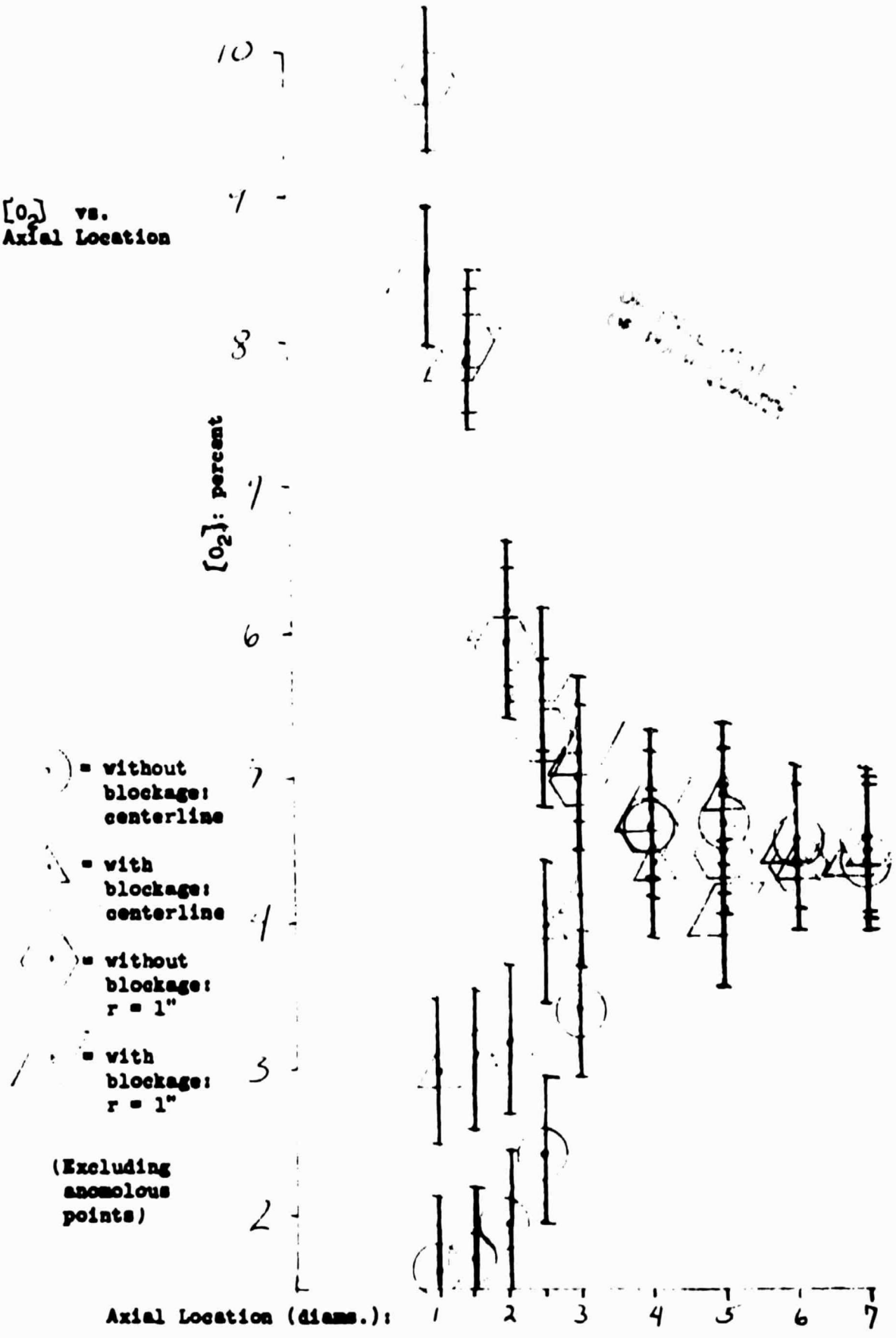

Fig. 19 The Variation of the Concentration of Oxygen at the Centerline of the Burner as a Function of Axial Location for Cases With and Without Blockage, Configuration D.

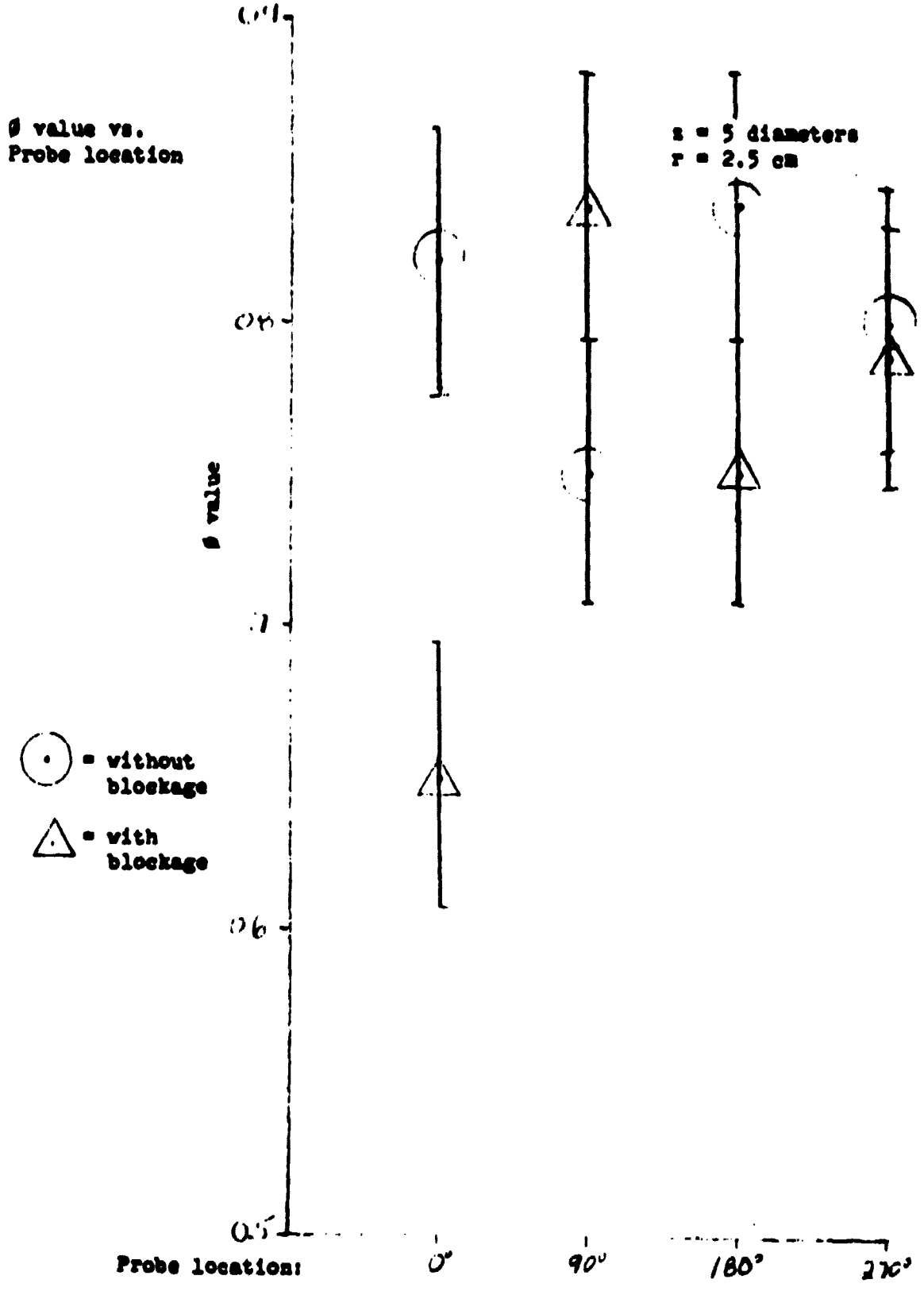

Fig. 20 Distribution of Equivalence Ratio in the Radial Plane Located at Five Diameters Downstream of the Injector for Cases With and Without Blockage, Configuration D.

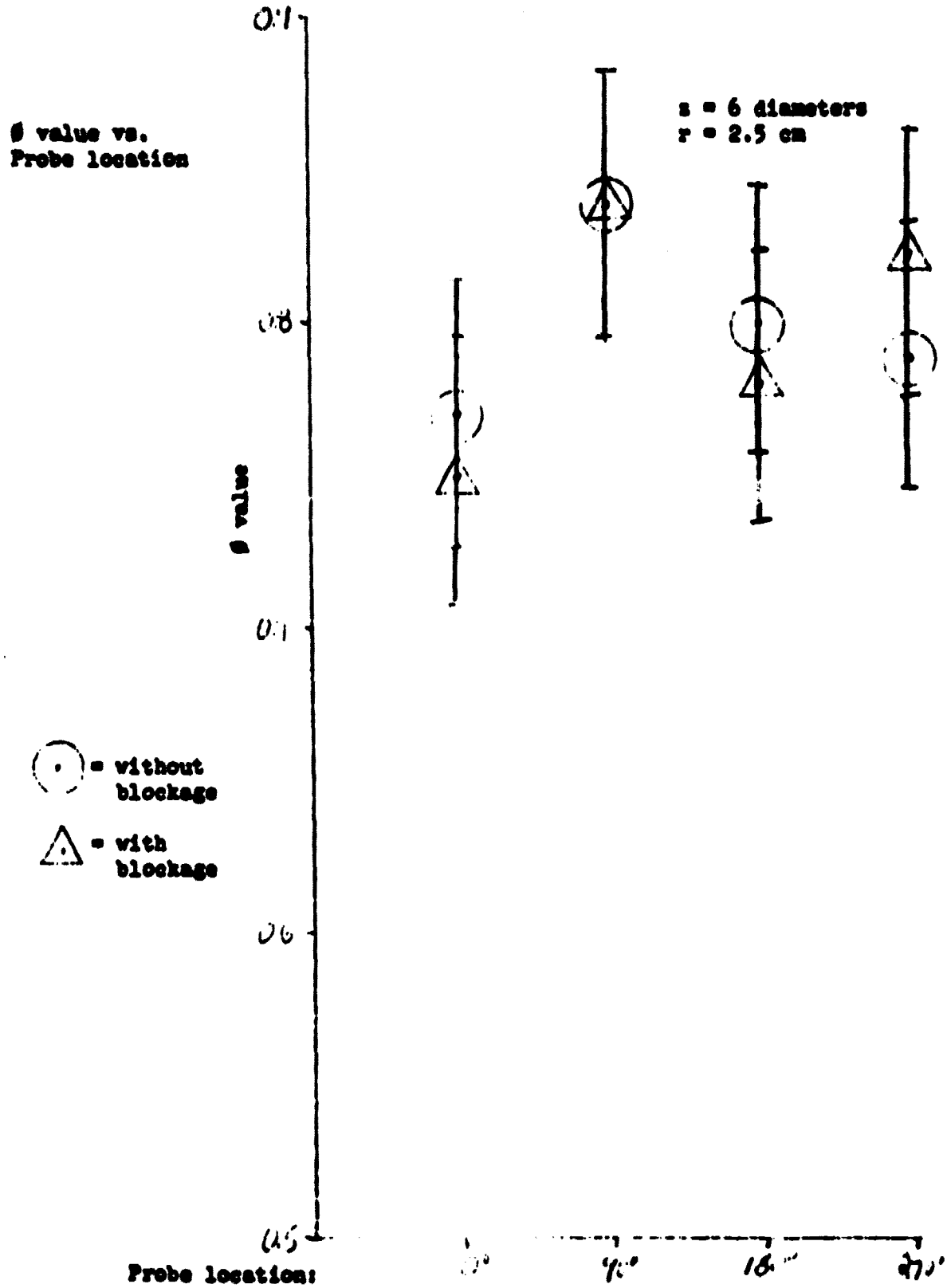

Fig. 21 Distribution of Equivalence Ratio in the Radial Plane Located at Six Diameters Downstream of the Injector for Cases With and Without Blockage, Configuration D.

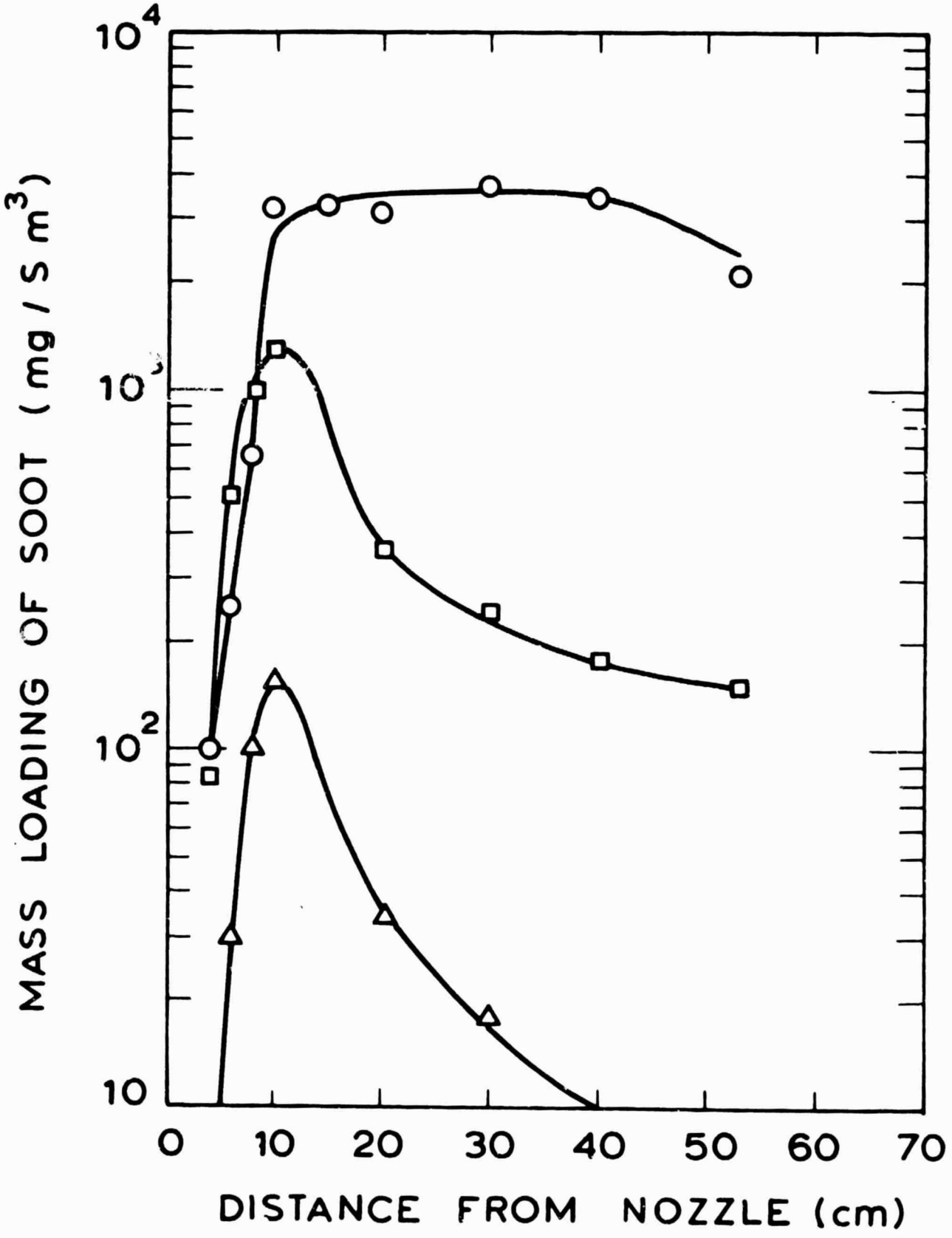

Fig. 22 Influence of Atomizing-Air Pressure on the Axial Profile of Soot Mass Loading. Kerosene/Air; Fuel Equivalence Ratio = 1.0; Cold Gas Velocity = .96 m/s; Atomizing-Air Pressure = (o) 184 KPa, (□) 205 KPa and (△) 239 KPa; Configuration A.

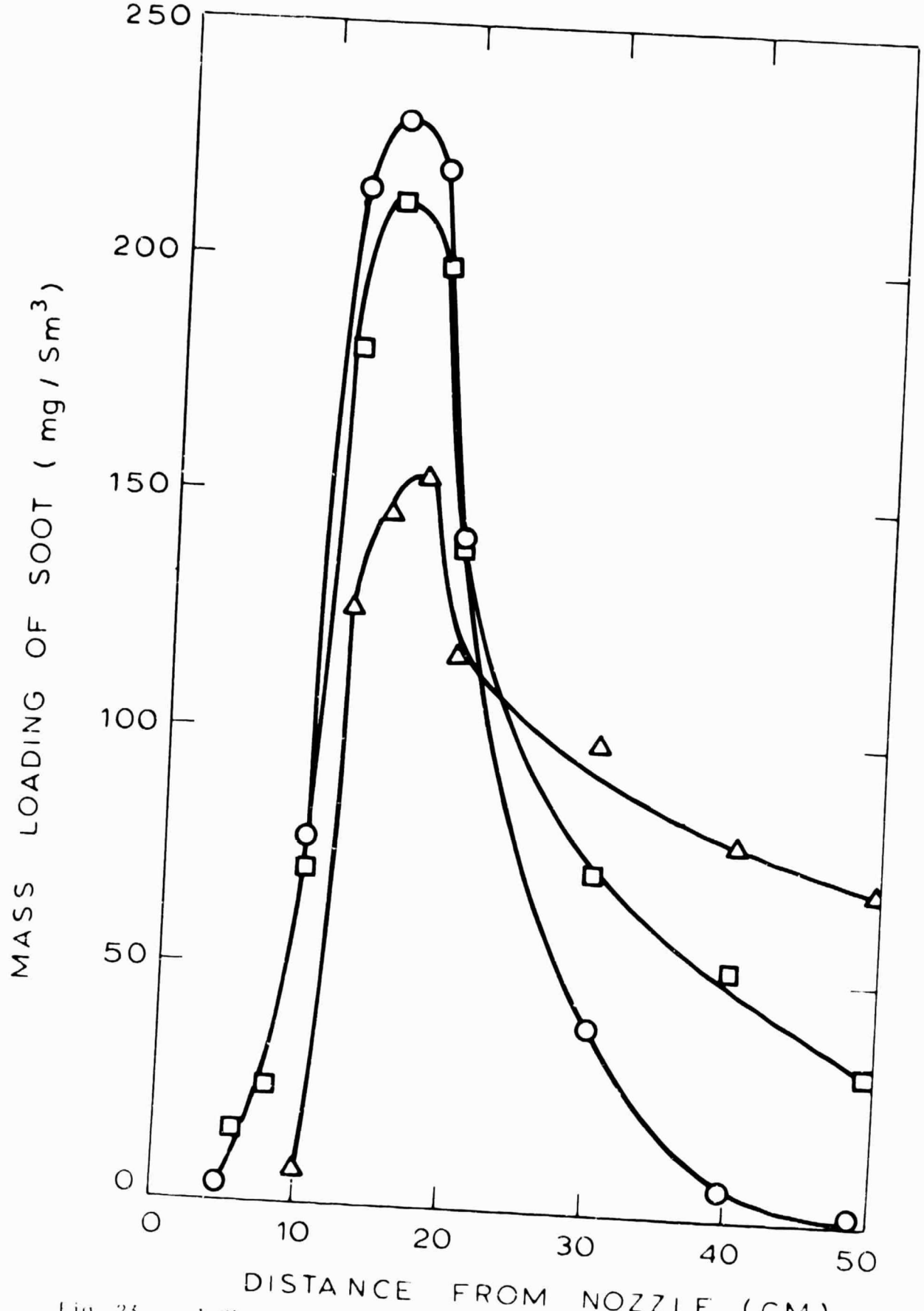

Fig. 23 Influence of Atomizing-Air Pressure on Axial Profile of Soot Mass Loading. Kerosene/air; Fuel Equivalence Ratio = 1.0, Cold Gas Velocity = 2.67 m/s; Atomizing-Air Pressure = (○) 184 KPa, (□) 205 KPa and (△) 239 KPa; Configuration B.

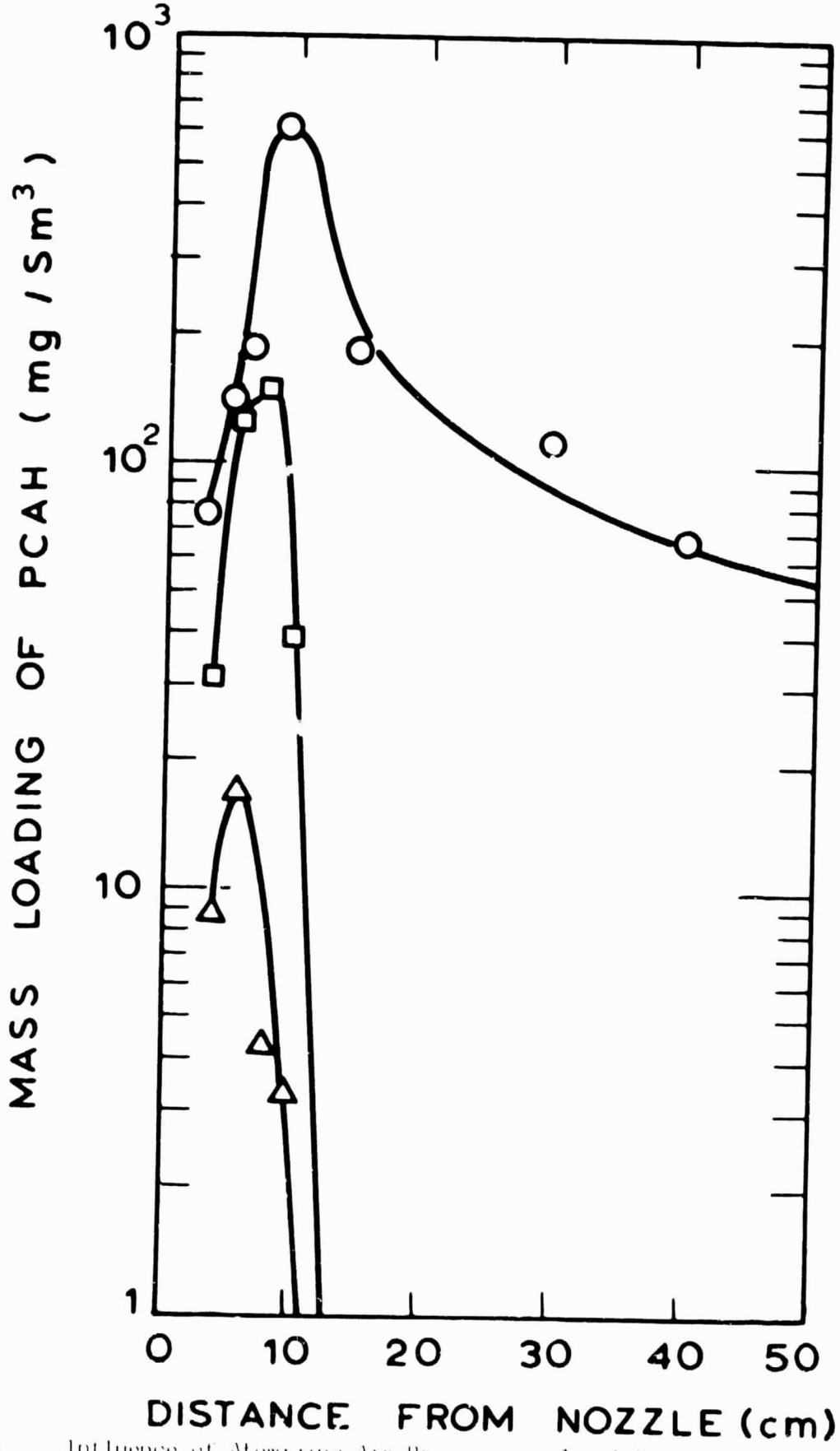

Fig. 24 Influence of Atomizing-Air Pressure on Axial Profile of PCAH Mass Loading. Kerosene/air; Fuel Equivalence Ratio = 1.0, Cold Gas Velocity = 0.96 m/s; Atomizing-Air Pressure = (O) 184 kPa, (□) 205 kPa, and (Δ) 239 kPa; Configuration A.

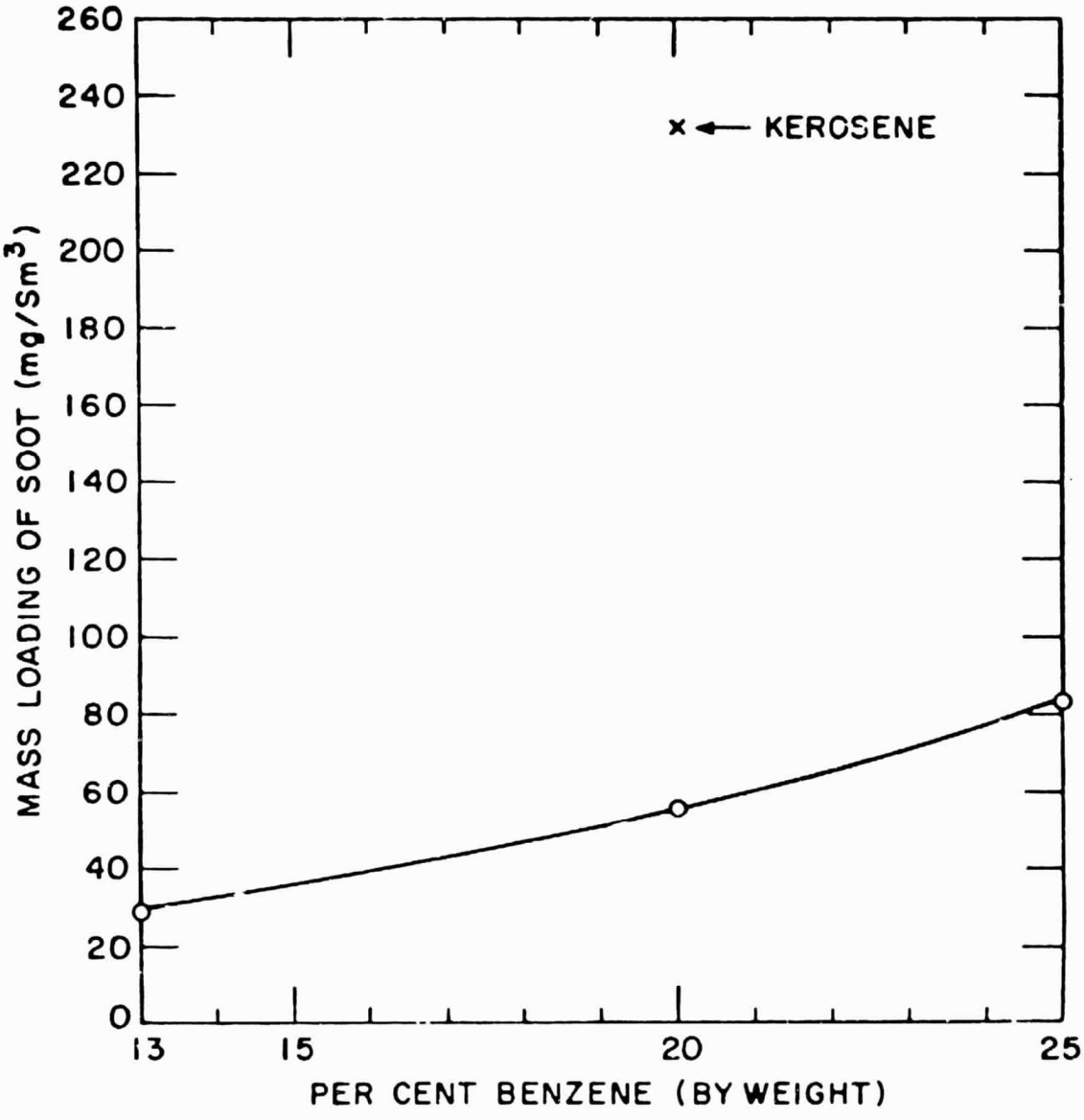

Fig. 25 Effect of Fuel Mixture (Benzene and Heptane) on the Peak Soot Concentration. Atomizing Pressure of 184 KPa, Axial Location of Measurements Two Burner Diameters Downstream of Injector, Configuration B.

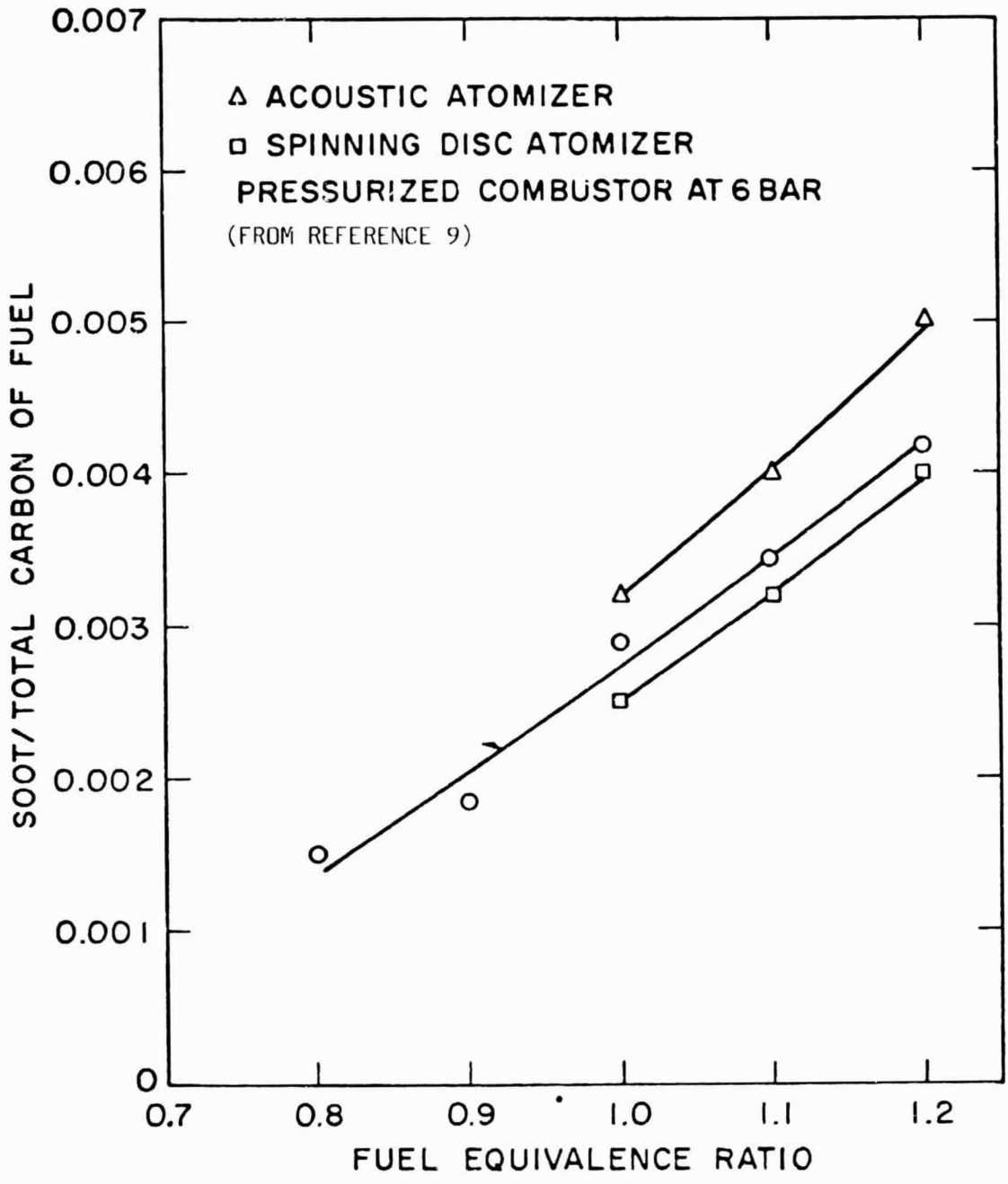

Fig. 26 Effect of Fuel Equivalence Ratio on Peak Soot Concentration (o) Kerosene/Air, Atomizing Pressure of 184 KPa, Axial location of Measurements Two Diameters Downstream of Injector, Configuration B; (△) and (□) Data from Holderness and MacFarlane, Reference 9.

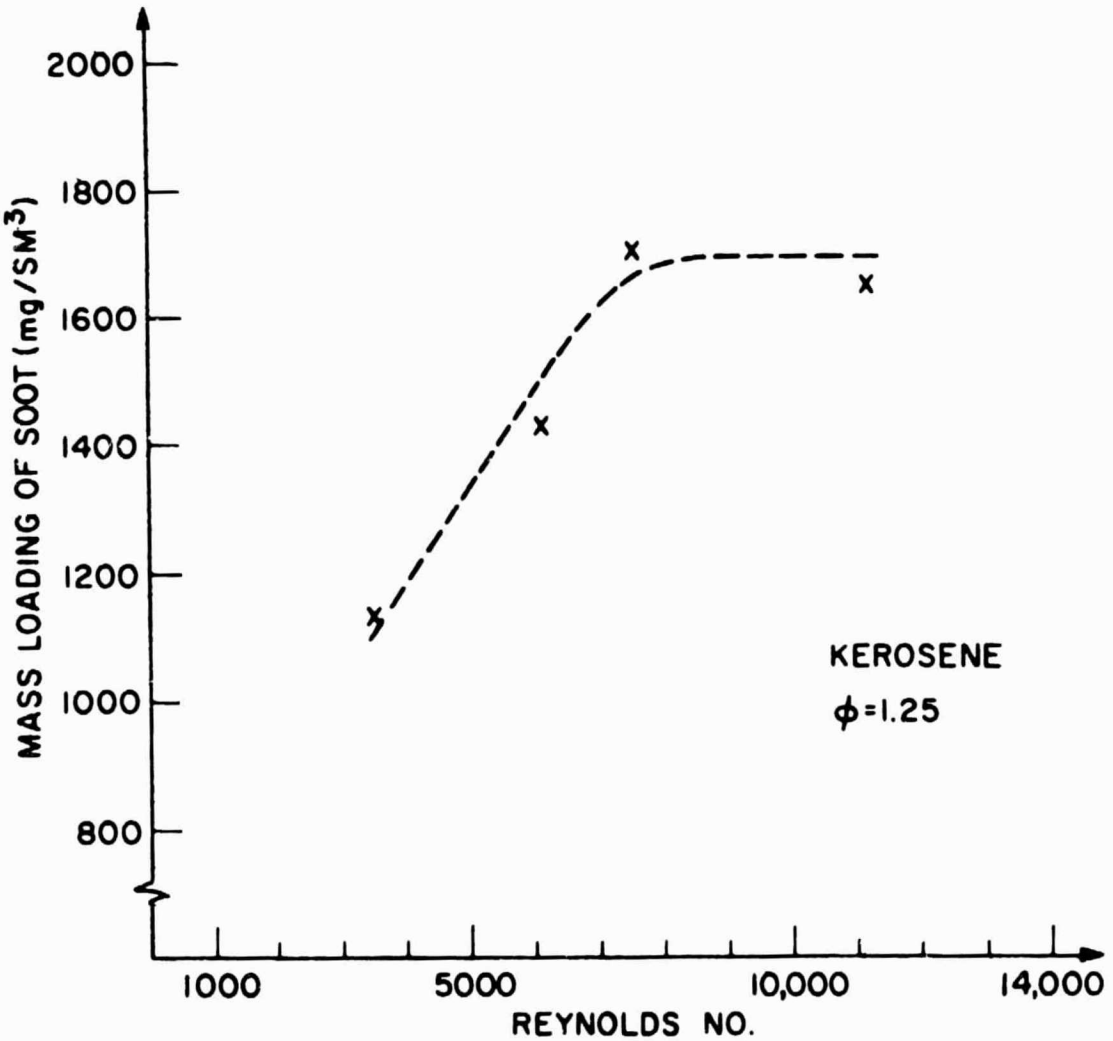

Fig. 27 Effect of Reynolds Number or Pressure on the Peak Soot Concentration. Kerosene/Air, Equivalence Ratio of 1.25, Atomizing Pressure 308 KPa, Configuration D.

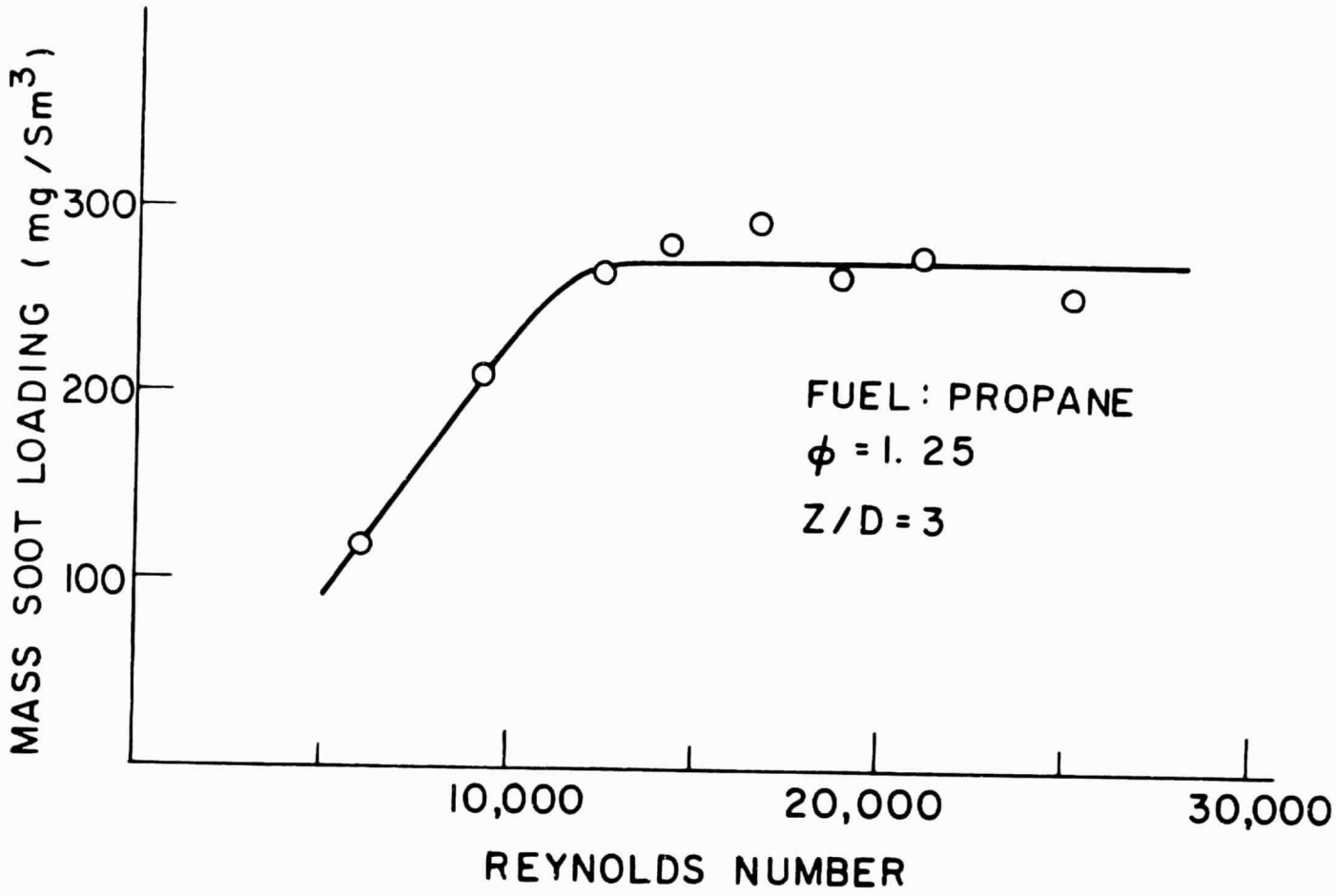

Fig. 28 Effect of Reynolds Number on Peak Soot Concentration from the Combustion of Propane, Configuration D.

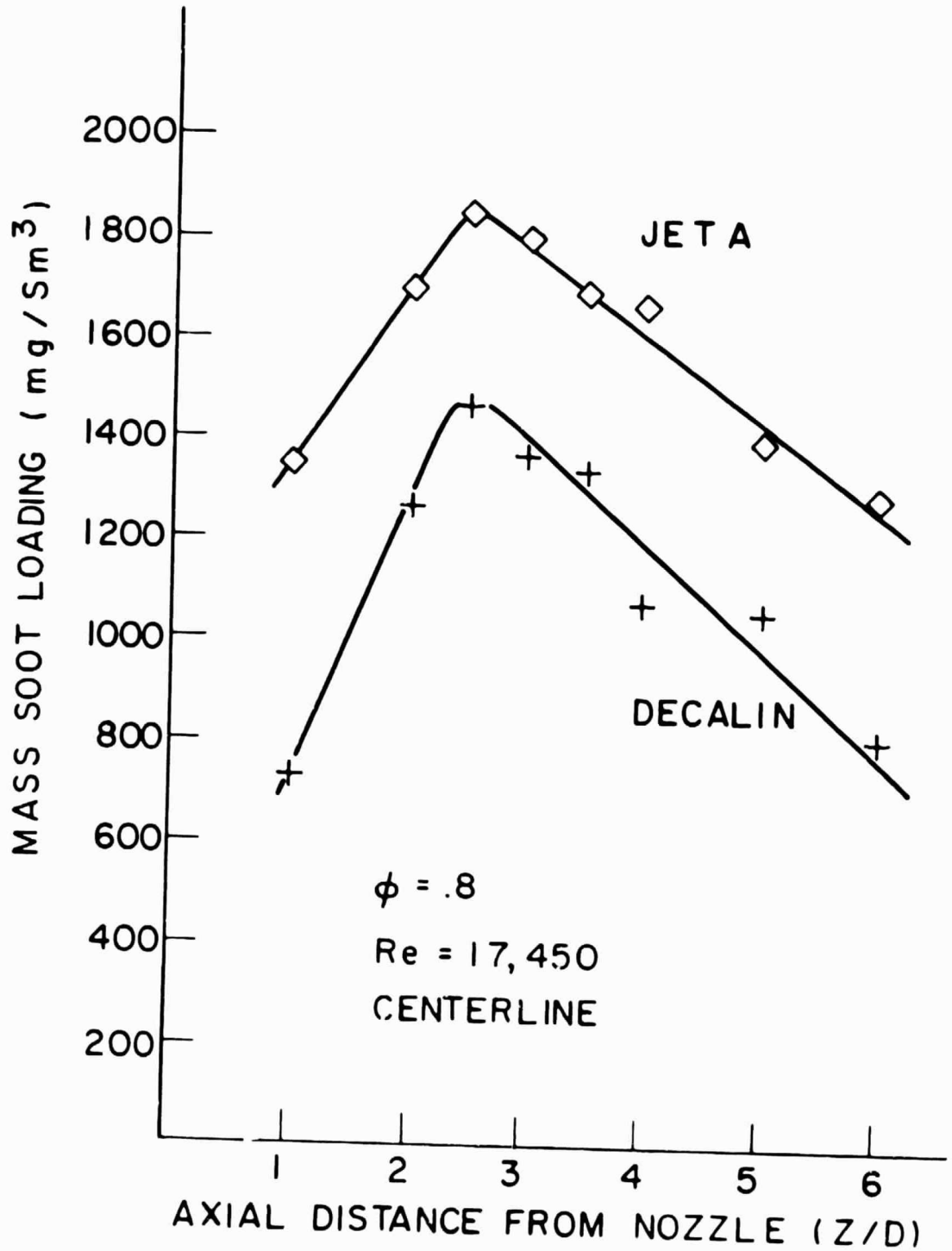

Fig. 29 Effect of Fuel Composition (Jet A and Decalin) on the Axial Profiles of Soot Concentration, Configuration D.

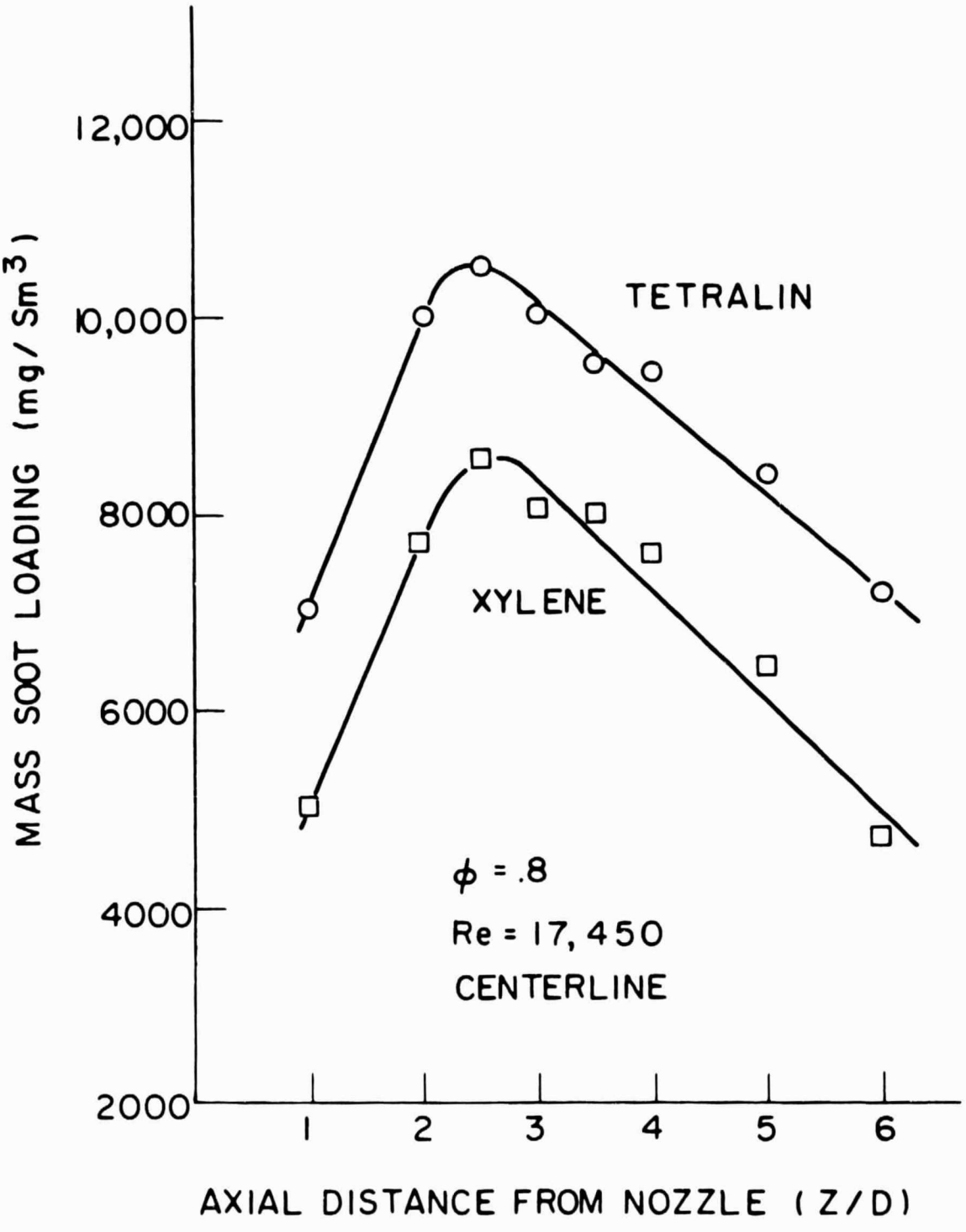

Fig. 30 Effect of Fuel Composition (Tetralin and Xylene) on Axial Profiles of Soot Concentration, Configuration D.

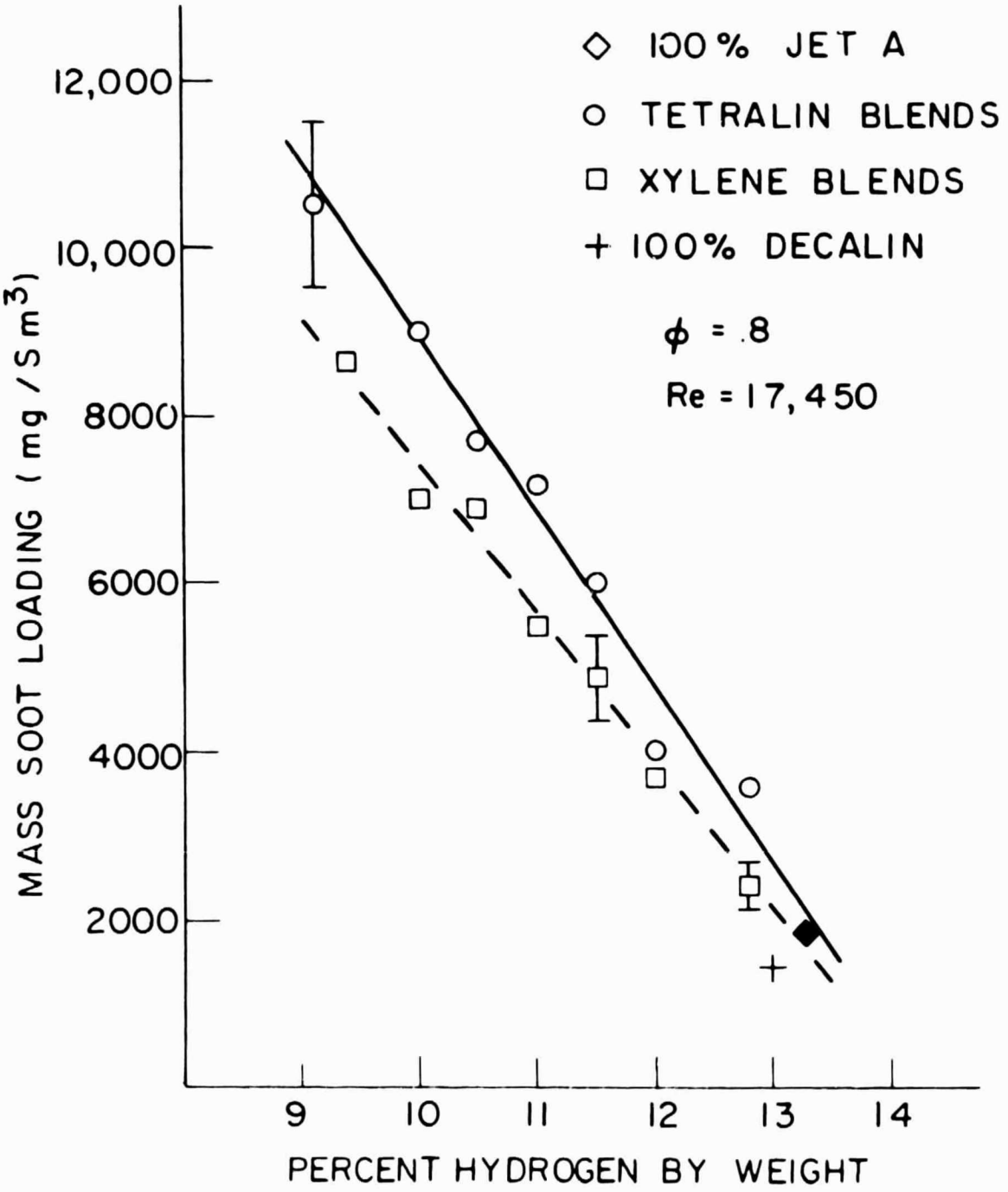

Fig. 31 Variation of Peak Soot Loading as a Function of the Percent of Hydrogen in the Fuel, Configuration D.